Onno Oncken
Guillermo Chong
Gerhard Franz
Peter Giese
Hans-Jürgen Götze
Victor A. Ramos
Manfred R. Strecker
Peter Wigger
(Editors)

The Andes

Active Subduction Orogeny

With 287 Figures, 159 in color

Frontiers in Earth Sciences
Series Editors: J. P. Brun, O. Oncken, H. Weissert, C. Dullo

Springer

Mechanism of the Andean Orogeny: Insight from Numerical Modeling

Stephan V. Sobolev · Andrey Y. Babeyko · Ivan Koulakov · Onno Oncken

Abstract. The Andes were formed by Cenozoic tectonic shortening of the South American plate margin overriding the subducting Nazca Plate. Using coupled, thermo-mechanical, numerical modeling of the dynamic interaction between subducting and overriding plates, we searched for factors controlling the intensity of the tectonic shortening. From our modeling, constrained by geological and geophysical observations, we infer that the most important factor was fast and accelerating (from 2 to 3 cm yr^{-1}) westward drift of the South American Plate, whereas possible changes in the convergence rate were not as important. Other important factors are the crustal structure of the overriding plate and the shear coupling at the plate interface.

The model in which the South American Plate has a thick (40–45 km at 35 Ma) crust and relatively high friction coefficient (0.05) at the Nazca-South American plate interface generates more than 300 km of tectonic shortening over the past 35 million years and replicates well the crustal structure and evolution of the high Central Andes. However, modeling does not confirm that possible climate-controlled changes to the sedimentary trench-fill during the last 30 million years might have significantly influenced the upper-plate shortening rate. The model with initially thinner (less than 40 km) continental crust and a lower friction coefficient (less than 0.015) results in less than 40 km of shortening in the South American Plate, replicating the situation in the Southern Andes.

During upper-plate deformation, the processes that cause a reduction in lithospheric strength and an increase in interplate coupling are particularly important. The most significant of these processes appears to be: (*1*) delamination of the lower crust and mantle lithosphere, driven by gabbro-eclogite transformation in the thickening lower crust, and (*2*) mechanical failure of the foreland sediments. The modeling demonstrates that delaminating lithosphere interacts with subduction-zone corner flow, influencing both the rate of tectonic shortening and magmatic-arc productivity, and suggests an anti-correlation between these two parameters. Our model also predicts that the down-dip limit of the frictional coupling domain between the Nazca and South American Plates should be ~15–20 km deeper in the Southern Andes (south of 28° S) compared to the high Central Andes, which is consistent with GPS and seismological observations.

25.1 Introduction and Key Questions

The South American Plate is drifting westwards, at a rate that has increased from ~2 to 3 cm yr^{-1} over the last 30 million years (Silver et al. 1998), over the Nazca Plate, which is subducting eastwards at about 5 cm yr^{-1} (Fig. 25.1). The Andean mountain belt stretches along the entire western margin of the South American Plate where it overlies the subducting Nazca Plate. There is a dramatic

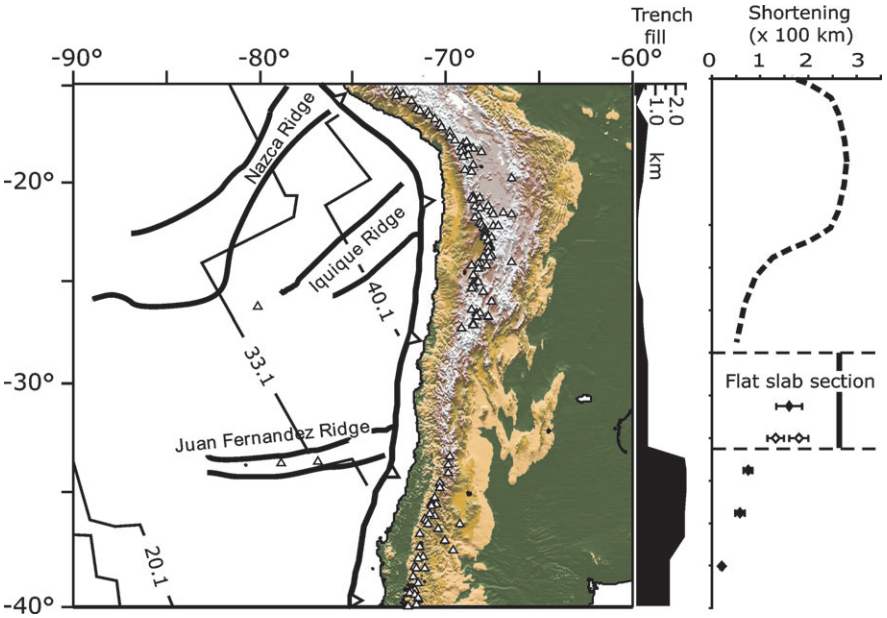

Fig. 25.1. Surface topography of the Andes, thickness of sedimentary trench-fill and magnitude of tectonic shortening. The trench adjacent to the high Central Andes, where the tectonic shortening is the largest, has no sedimentary fill, which might increase friction in the subduction channel (Lamb and Davis 2003)

difference between the central part (~17–27° S) and the rest of the Andes. The Altiplano-Puna Plateau of the Central Andes is the second greatest plateau in the world (after Tibet) and has an average elevation of about 4 km and an area of more than 500 000 km^2 (Fig. 25.1). The plateau has resulted from up to 300 km of late Cenozoic, crustal shortening at the western edge of the South American Plate. This shortening generated unusually thick, hot and felsic, continental crust (Isacks 1988; Allmendinger and Gubbels 1996, Allmendinger et al. 1997; Lamb et al. 1997; Kley and Monaldi 1998; Giese et al. 1999; Lucassen et al. 2001; Yuan et al. 2002; Beck and Zandt 2002; Lamb and Davis 2003). In contrast to the Central Andes, no high plateau exists in the Northern and Southern Andes (Fig. 25.1), where only minor (less than 50 km) tectonic shortening has been reported (e.g., Allmendinger et al. 1997; Lamb et al. 1997; Kley and Monaldi 1998). The tectonic shortening was not only much less intensive in the Southern Andes than in Central Andes but also started much later (Vietor and Echtler 2006, Chap. 18 of this volume).

In addition to this first-order difference between the central and Southern Andes, somewhat subordinate, although still very important, is the difference between the structure and deformation style in the Altiplano and Puna segments of the Central Andes (Allmendinger and Gubbels 1996; Kley and Monaldi 1998). North of 23° S, in the Altiplano segment, the tectonic shortening started early (at about 50 Ma) and was most intensive during the last 10 million years, forming a broad, thin-skinned Subandean thrust belt. South of 23° S, in the Puna, tectonic shortening started later, was much less intense and generated a thick-skinned deformation pattern (Allmendinger and Gubbels 1996; Kley and Monaldi 1998).

Perhaps the key question about Andean orogeny is why the high plateau has developed only in the Central Andes and only in Cenozoic times (mostly during the last 30 million years), even though the Nazca Plate has been subducting along the entire western margin of South America for more than the last 200 million years (e.g., Isacks 1988; Allmendinger et al. 1997; see Oncken et al. 2006, Chap. 1 of this volume, for a review of the deformation history of the Central Andes).

Several ideas have been proposed in answer to this question. Isacks (1988) suggested that before about 25–30 Ma, large parts of the Central Andes were underlain by a shallow-dipping slab that became steeper at ~25 Ma, causing thermal weakening and intensive tectonic shortening in the compressed lithosphere of the overriding plate. In another hypothesis (Mégard et al. 1984; Pardo-Casas and Molnar 1987; Somoza 1998), the beginning of intensive tectonic shortening in the Andes was associated with major reorganization of plate motion followed by an increase in the Nazca-South American convergence rate at ~25–30 Ma. Russo and Silver (1994) attributed the Andean orogeny to the Cenozoic increase in the westward drift rate of the South American Plate and associated mantle flow, whose north-south heterogeneity determined the difference in the intensity of deformation between the center and the rest of the Andes. Lamb and Davis (2003) proposed that the high shear stress at the interface between the Nazca and South American Plates, caused by sediment starvation in the Central Andean trench, was crucial for the deformation of the upper plate. Based on the correlation between the shortening rate in the Central Andes and the global temperature of the ocean, these authors have also suggested that this sediment starvation was caused by global climate change beginning at 30 Ma and, therefore, climate was the sole factor responsible for the formation of high Andes.

In relation to the different deformation styles of the Altiplano and Puna segments of the Central Andes, Allmendinger and Gubbels (1996) noticed the striking correlation between the deformation styles and the distribution of thick, Paleozoic, sedimentary basins. These basins are abundant in the foreland of the Altiplano but absent in the foreland of the Puna. Another clear difference in the lithospheric structure beneath the Puna and Altiplano segments are the much higher seismic-wave attenuation and seismic velocities beneath the Puna region (Whitman et al. 1996; Koulakov et al. 2006), indicating significant north-south variations in lithospheric temperature and, hence, in the mechanical strength of the foreland. These observations suggest that the shortening style of the whole system might be controlled by lateral, north-to-south variation in the mechanical properties of the lithosphere.

Another key question related to the Andean orogeny is what happened to the mantle lithosphere under the plateau. A simple argument of mass conservation suggests that the entire lithosphere must be doubled in the places where the crustal thickness has also been tectonically doubled. The consequence would be low crustal temperature and reduced surface heat flow for at least a few tens of millions of years (e.g., Babeyko et al. 2002). However, this contradicts the high values of surface heat flow in the Altiplano (Springer and Förster 1998) and the evidence of partial melting in the Altiplano mid-crust (Yuan et al. 2000). Kay and Kay (1993) suggested that the mantle lithosphere might have been delaminated, but found evidence for this process only for the Puna Plateau and not for the Altiplano. Pope and Willet (1998) postulated the ablative subduction scenario for the Central Andes in which the thickening mantle lithosphere of the upper plate was eroded by the subducting plate. However, this condition was kinematically predefined in their model and, to date, its validity has not been tested by a dynamic model.

Another striking feature of the Andean orogeny is the remarkable correlation between surface topography and the dip of the slab, and their symmetry with the symmetry axis at ~19° S (Gephart 1994), at the so-called Boliv-

ian orocline. Based on these observations, Gephart (1994) stated that the relationship between these parameters suggests that the surface topography of the Andes strongly depends on subduction dynamics, but he did not specify a mechanism.

The diversity of the suggested hypotheses reflects the complexity of the deformation processes responsible for the Andean orogeny, and also indicates the lack of quantitative understanding of these processes. One way to improve such understanding is to study the temporal correlation between tectonic shortening and those processes that possibly contribute to the deformation of the upper plate (Oncken et al. 2006, Chap. 1 of this volume). Such analyses show that the shortening rate in the Central Andes correlates well with the westward drift velocity of the South American Plate, whereas it does not correlate with the convergence rate between the Nazca and South American Plates. As mentioned above, the shortening rate also correlates well with the global ocean temperature (Lamb and Davis 2003; Oncken et al. 2006, Chap. 1 of this volume), apparently suggesting a strong relationship between the Andean orogeny and changing global climate (Lamb and Davis 2003). However, close examination of this issue using geological arguments (Oncken et al. 2006, Chap. 1 of this volume) and our modeling results, presented below, suggest an illusive character to this relationship, reminding us that good correlation between processes does not necessarily mean there is a genetic relationship.

We believe that the best way to understand complicated deformation processes at the active continental margin is by using advanced physical-mathematical modeling that is constrained by robust geological and geophysical observations. In this study, we used finite-element numerical modeling to consider the coupled, thermo-mechanical, dynamic interaction between the subducting and overriding plates over a few tens of millions of years at the spatial scale of the upper mantle. We studied mass and heat fluxes associated with this interaction, particularly focusing on the dependence of tectonic deformation in the overriding plate on: (*1*) convergence rate; (*2*) overriding rate; (*3*) strength of mechanical coupling between subducting and overriding plates; and (*4*) initial lithospheric structure. We derived models consistent with observations of the central and Southern Andes and defined key predictions of these models. Finally we suggest our preferred scenario for the Andean orogeny.

25.2 Method and Model Set-Up

According to the aim of this study, the temporal scale for our modeling is a few tens of millions of years and the spatial scale is 1 000 km. Long-term temporal analysis requires that we fully consider coupled, thermo-mechanical processes. Moreover, modeling the dynamic interaction between subducting and overriding plates demands realistic rheological models of both plates, including elasticity, plasticity, as well as temperature- and stress-dependent viscosity. Modeling of this type, and at this scale, is exceptionally difficult and is not yet possible in three dimensions. Therefore, we have exploited the fact that the variation in structure parallel to the strike of the Andes is much smaller than across strike, which enabled the deformation processes to be modeled with practically independent, two-dimensional (2D) cross sections oriented perpendicular to the strike of the Andes.

25.2.1 Basic Equations

The deformation process was modeled by numerical integration of the fully coupled system of 2D conservation equations for momentum (Eq. 25.1), mass (Eq. 25.2) and energy (Eq. 25.3). These equations are solved together with rheological relations (Eqs. 24.4 and 25.5) including those for a Maxwell visco-elastic body with temperature- and stress-dependent viscosity (Eq. 25.4), and a Mohr-Coulomb failure criterion with non-associated (zero dilation angle), shear flow potential (Eq 25.5). It was assumed that viscous deformation consists of competing dislocation, diffusion and Peierls creep mechanisms (Kameyama et al. 1999).

$$-\frac{\partial p}{\partial x_i}+\frac{\partial \tau_{ij}}{\partial x_j}+\rho g_i=0,\quad i=1,2 \tag{25.1}$$

$$\frac{1}{K}\frac{\mathrm{d}p}{\mathrm{d}t}-\alpha\frac{\mathrm{d}T}{\mathrm{d}t}=-\frac{\partial v_i}{\partial x_i} \tag{25.2}$$

$$\rho C_\mathrm{p}\frac{\mathrm{d}T}{\mathrm{d}t}=\frac{\partial}{\partial x_i}\left(\lambda(x_i,T)\frac{\partial T}{\partial x_i}\right)+\tau_{ij}(\dot{\varepsilon}^\mathrm{v}_{ij}+\dot{\varepsilon}^\mathrm{p}_{ij})+\rho A \tag{25.3}$$

$$\frac{1}{2G}\frac{\hat{\mathrm{d}}\tau_{ij}}{\mathrm{d}t}+\frac{1}{2\eta}\tau_{ij}+\dot{\varepsilon}^\mathrm{p}_{ij}=\dot{\varepsilon}_{ij} \tag{25.4}$$

$$\frac{1}{\eta(\tau,T)}=\frac{1}{\eta_\mathrm{dif}(T)}+\frac{1}{\eta_\mathrm{dis}(\tau,T)}+\frac{1}{\eta_\mathrm{p}(\tau,T)}$$

$$\sigma_1-\sigma_3\frac{1+\sin\phi}{1-\sin\phi}+2c\sqrt{\frac{1+\sin\phi}{1-\sin\phi}}=0 \tag{25.5}$$

$$g_\mathrm{s}=\sigma_1-\sigma_3$$

Here the Einstein summation convention applies and x_i are coordinates, t – time, v_i – velocities, p – pressure, τ_{ij} and $\dot{\varepsilon}_{ij}$ – stress and strain-rate deviators, $\dot{\varepsilon}^\mathrm{v}_{ij}$ and $\dot{\varepsilon}^\mathrm{p}_{ij}$ are viscous and plastic strain-rate deviators, respectively, $\mathrm{d}/\mathrm{d}t$ – convective time derivative, $\hat{\mathrm{d}}\tau_{ij}/\mathrm{d}t$ – Jaumann co-rotational deviatoric stress rate, ρ – density, g_i – gravity

vector, K and G – bulk and shear moduli, η – viscosity, η_{dif} – diffusion creep viscosity, η_{dis} – dislocation creep viscosity, η_P – Peierls creep viscosity, τ – square root of second invariant of stress tensor, R – gas constant, T – temperature, σ_1, σ_3 – maximal and minimal principal stresses, ϕ – angle of friction, c – cohesion, g_s– shear plastic flow potential, C_p – heat capacity, λ – heat conductivity, and A – radioactive heat production.

25.2.2 The Plate Interface and Gabbro-Eclogite Transformation

The interface between the slab and the upper plate was modeled as a 12 km-thick subduction channel with plastic rheology using three finite elements (two elements for the oceanic-slab side and one element for the continental-plate side). The yield stress was defined as the smallest of either the (Mohr-Coulomb) frictional stress:

$$\tau = c + \mu \sigma_n \tag{25.6}$$

or the temperature-dependent, viscous shear stress (Peacock 1996):

$$\tau = \tau_0 \exp\left(-\frac{T - T_0}{\Delta T}\right) \tag{25.7}$$

In both equations, τ is a stress norm defined as the square root of the second invariant of the stress tensor, c is cohesion, σ_n is normal stress, μ is the subduction-channel, effective friction coefficient, which includes the effect of fluid pressure, T and T_0 are local and reference temperatures, and τ_0 and ΔT are parameters. The parameters of Eq. 25.7, T_0, ΔT and τ_0, are assumed to be 400 °C, 75 °C and 60 MPa, respectively, close to the values of Peacock (1996).

With this approach, the shallow, low-temperature part of the subduction channel has frictional (brittle) rheology with shear stress increasing with depth (Fig. 25.2, *solid* and *dashed curves*). At greater depth and higher temperature, the viscous flow mechanism takes over and shear stress in the channel decreases with depth (Fig. 25.2, *solid curve*). The depth where frictional rheology changes to viscous rheology depends on the friction coefficient and it is larger where friction is lower (compare *dashed* and *solid curves* in Fig. 25.2). We considered the friction coefficient in the subduction channel as a model parameter and changed it from 0 to 0.15, which is in agreement with previous estimates (Bird 1998; Tichelaar and Ruff 1993; Peacock 1996; Hassani et al. 1997).

We also took into account gabbro-eclogite transformation in both oceanic crust and continental lower crust. For simplicity, we used the same gabbro-eclogite phase diagram for both crusts, calculated for the average gabbro composition using the free Gibbs energy minimization technique (Sobolev and Babeyko 1994) and do not consider neither related volume changes nor latent heat effects. The density of the eclogite (at room conditions) was set to 3450 kg m^{-3} and, in all models, the kinetic blocking temperature for the gabbro-eclogite transforma-

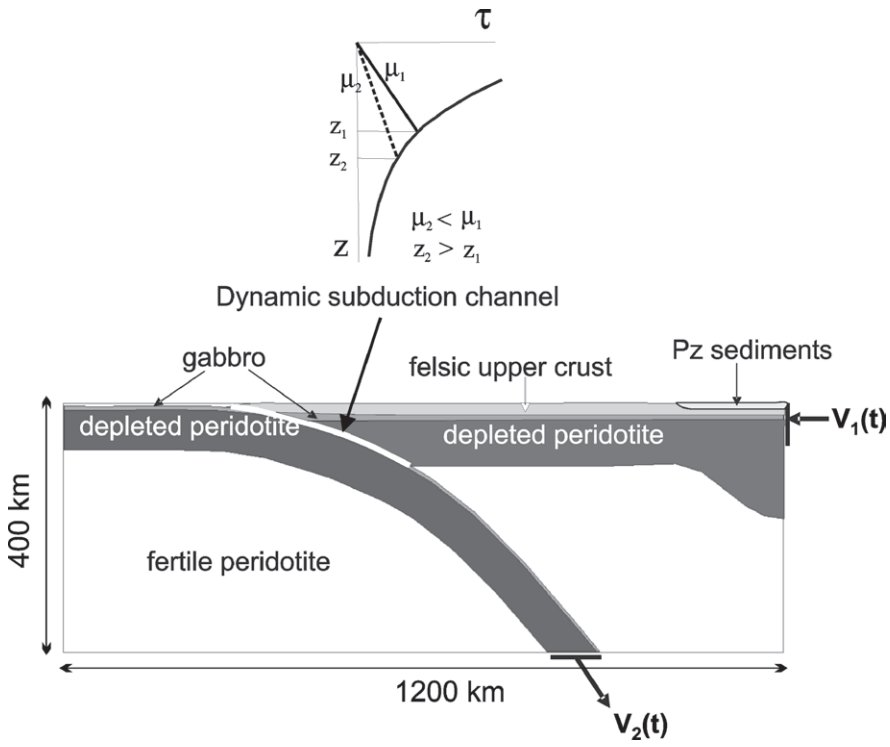

Fig. 25.2.
Model set-up and boundary conditions. The subducting plate is 45 million years old. The initial thickness of the continental lithosphere is 100–130 km, with the thickest lithosphere in the eastern (right) part of the model corresponding to the Brazilian Shield margin. South America is drifting to the west (left) with the velocity increasing from 2 to 3 cm yr^{-1} during the last 35 million years. The lower end of the Nazca Plate is pulled down with the velocity changing from 5 to 13 cm yr^{-1}. The inlet shows the shear stress in the subduction channel. Note that with a lower friction coefficient in the channel, the friction (brittle) domain extends deeper

tion was 800 °C for the oceanic crust and 700 °C for the lower continental crust. We do not consider here the details of the processes in the fore-arc. Therefore we omit a number of hydration and dehydration reactions in the subducting lithosphere (see Poli and Schmidt 2002; Hacker et al. 2003 for reviews), which lead to interesting geodynamic consequences at the fore-arc scale (Gerya et al. 2002; Gerya and Yuen 2003).

25.2.3 Numerical Method and Rheology

We integrated Eqs 25.1–25.7 using a 2D, parallel, thermomechanical, finite-element/finite-difference code called "LAPEX-2D" (Babeyko and Sobolev 2005; Sobolev and Babeyko 2005; see also Babeyko et al. 2002, for a description of the previous version of the code). This code combines the explicit Lagrangian algorithm FLAC (Polyakov et al. 1993; Cundall and Board 1988) with the particle technique that is similar to the particle-in-cell method (Sulsky et al. 1995; Moresi et al. 2001). Particles track material properties and the full stress tensor, thereby minimizing numerical diffusion related to re-meshing. The method allows the employment of realistic temperature- and stress-dependent, visco-elastic rheology combined with Mohr-Coulomb plasticity for layered oceanic and continental lithosphere (Fig. 25.2).

The rheological parameters were taken from published experimental and theoretical studies and are presented in Table 25.1. Owing to the presence of the subduction zone, we have used rheological parameters for "wet" rocks everywhere in the model except for the slab and mantle lithosphere of the shield margin. In the crust, we employed friction and viscosity strain softening, which we assumed to be more intensive in the Paleozoic sediments of the Subandean Zone (Fig. 25.2). The viscous deformation in the mantle was considered to be driven by competing dislocation, diffusion and Peierls creep mechanisms (Kameyama et al. 1999) and the numerical method routinely included shear heating.

At high strains, rocks may mechanically weaken owing to a number of processes (Handy et al. 1999). We considered this in the model by introducing plastic and viscous strain-softening behavior. For felsic and mafic continental rocks, we assumed that cohesion and friction angles

Table 25.1. Material parameters

Parameter	Sediments	Felsic crust	Gabbro continent/ocean	Mantle lithosphere of slab and shield	Mantle lithosphere/asthenosphere
Density at room conditions, ρ (kg m^{-3})[a]	2 670	2 800	3 000	3 280	3 280/3 300
Thermal expansion, α (K^{-1})[b]	3.7×10^{-5}	3.7×10^{-5}	2.7×10^{-5}	3.0×10^{-5}	3.0×10^{-5}
Elastic moduli, K, G (GPa)[b]	55, 36	55, 36	63, 40	122, 74	122, 74
Heat capacity, C_p (J kg^{-1} K^{-1})[b]	1 200	1 200	1 200	1 200	1 200
Heat conductivity, λ (W K^{-1} m^{-1})	2.5	2.5	2.5	3.3	3.3
Heat productivity, A (μW m^{-3})	1.3	1.3*	0.2	0	0
Initial friction angle, ϕ (degree)	30	30	30	30	30
Initial cohesion, C_h (MPa)	2	20	40	40	40
Diffusion creep preexp. factor, log(A) (Pa^{-n} s^{-1})	–	–	–	–10.59	–10.59
Diffusion creep activation energy (kJ mol^{-1})	–	–	–	300	300
Grain size (mm), (Grain size exponent)	–	–	–	0.1 (2.5)	0.1 (2.5)
Dislocation creep preexp. factor, log(A) (Pa^{-n} s^{-1})	–28.0	–28.0	–15.4/–25.9	–16.3	–14.3
Dislocation creep activation energy (kJ mol^{-1})	223	223	356/485	535	515
Power law exponent, n	4.0	4.0	3.0/4.7	3.5	3.5
Peierls creep preexp. factor, log(A) (Pa^{-n} s^{-1})					
Peierls stress, σ_P (GPa)	–	–	–	8.5	8.5
Peierls creep activation energy (kJ mol^{-1})	223	223	445	535	535

[a] (Lukassen et al. 2001). [b] (Sobolev and Babeyko 1994). Sources for dislocation creep laws – sediments and felsic crust: weakened (A increased by 10 times) quartzite by Gleason and Tullis (1995); mafic crust of continent: wet plagioclase by Rybacki and Dresen (2000); mafic crust of ocean: dry Columbian basalt by Mackwell et al. (1998); mantle lithosphere of slab and shield: dry peridotite by Hirth and Kohlstedt (1996); mantle lithosphere of South America (except shield) and asthenosphere: dry peridotite by Hirth and Kohlstedt (1996). Source for diffusion and Peierls creep laws in mantle: Kameyama et al. (1999).

linearly decrease by a factor of three when accumulated plastic strain changes from 1 to 2. For sediment, the softening was assumed to be faster; the friction angle decreases by a factor of ten when the accumulated plastic strain changes from 0 to 0.5. The viscosity of all continental crustal materials was assumed to decrease by a factor of ten (log linearly) when finite strain changes from 0.5 to 1.0.

25.2.4 Model Set-Up

We modeled the initial crustal structures expected for the central and Southern Andes at 35 Ma. The initial crustal structure for the Central Andes (Fig. 25.4a) contains thick, felsic, upper crust and thinner, mafic, lower crust, with a total crustal thickness of 40–45 km, assuming that the crust was already significantly shortened by 35 Ma (Allmendinger et al. 1997; Lamb et al. 1997). The initial crust for the Southern Andes (see below Fig. 25.4c) consists of equally thick, upper felsic and lower mafic layers and has a total thickness of 35–40 km.

The geometry and boundary conditions incorporated into all our models are schematically shown in Fig. 25.2. In all models, we explored the interaction of the 45 million-year-old, subducting Nazca Plate with the 100 to 130 km-thick lithosphere of the overriding South American Plate during the last 35 million years. Relatively thin (100 km) lithosphere of the South America plate margin between the magmatic arc and Brazilian Shield margin is consistent with the concept of weak lithosphere of the back-arc mobile belt (Hyndman et al. 2005). Initial lithosphere of Brazilian Shield margin was taken to be 130 km. We assumed also a rather low-angle geometry for the subducting plate, consistent with the present-day structure in the Andes. The model box was 1 200 km long and 400 km high (Fig. 25.2) and moved to the left (west) together with the overriding plate. The drift of the overriding plate and subduction were generated by pushing the overriding plate at its right boundary and by pulling the slab from below, with the velocities taken from plate-tectonics reconstructions (Somoza 1998; Silver et al. 1998). In this approach, velocity boundary conditions move together with the overriding plate (push) and the retreating slab (pull). All other parts of the model box boundary were open for the free motion of material. The surface was treated as a stress free boundary and lower boundary as an open Winkler foundation boundary. Temperature was constant at the surface (0 °C) and at the lower boundary (1 350 °C). At the left and right boundaries horizontal heat flow was assumed to be 0.

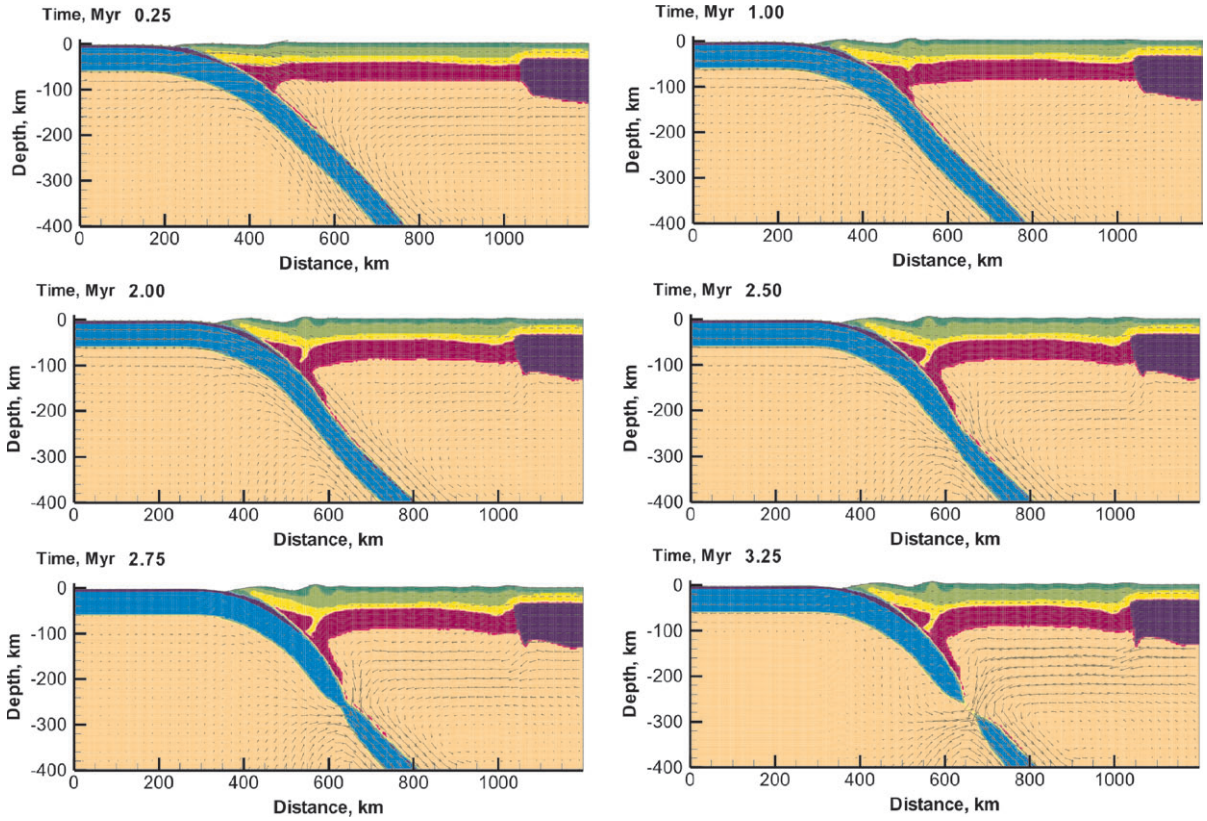

Fig. 25.3. Evolution of the slab in the model with high interplate friction coefficient (0.10). Colors represent rock types and vectors show velocity vectors. At $t = 3$ Myr the slab (*blue*) breaks off. The similar picture is observed at interplate friction coefficients higher than 0.10

25.3 Modeling Results

25.3.1 Model for the Central Andes (Latitude of the Altiplano)

Firstly, we sought the model that best fits the observations from the Central Andes (latitude of the Altiplano) for the time between 35 Ma to the present day. To do that, we assumed thick (40–45 km) crust as a starting model and used kinematic boundary conditions that mimicked subduction and overriding velocities according to the plate-tectonics reconstructions (Somoza 1998; Silver et al. 1998), as shown in Fig. 25.2. With this set-up, we performed several numerical experiments by changing the friction coefficient in the subduction channel "μ". All model-runs with $\mu > 0.10$ resulted in slab break-off and the termination of subduction (Fig. 25.3, see also animation 1 on the Supplementary DVD). When μ was in the range of 0.05–0.10, subduction survived but large interplate coupling led to shortening in the overriding plate that was too strong.

The model replicates the case of the Central Andes most closely when μ is about 0.05 (Fig. 25.4b). In this model, 58% of the westward drift of South America during the last 35 million years is accommodated by trench roll-back and the remaining 42% by tectonic shortening (37%) and subduction erosion (5%) of the South American margin. During shortening, the felsic crust almost doubled its thickness, while the thickness of the mafic lower crust and mantle lithosphere actually reduced (compare Fig. 25.4a,b). The reason for this is delamination of the lower crust and mantle lithosphere driven by gabbro-eclogite transformation in the lower crust, first discussed in the Andean context by Kay and Kay (1993).

During the thickening of the crust to more than 45 km, the mineral reactions in the mafic lower crust generated dense garnet and omphacite at the expense of low-density plagioclase, thus increasing the rock density to values higher than that of mantle peridotite (3 300 kg m^{-3}). The bodies of the dense lower crust and entrained mantle lithosphere tend to sink into the less dense asthenosphere.

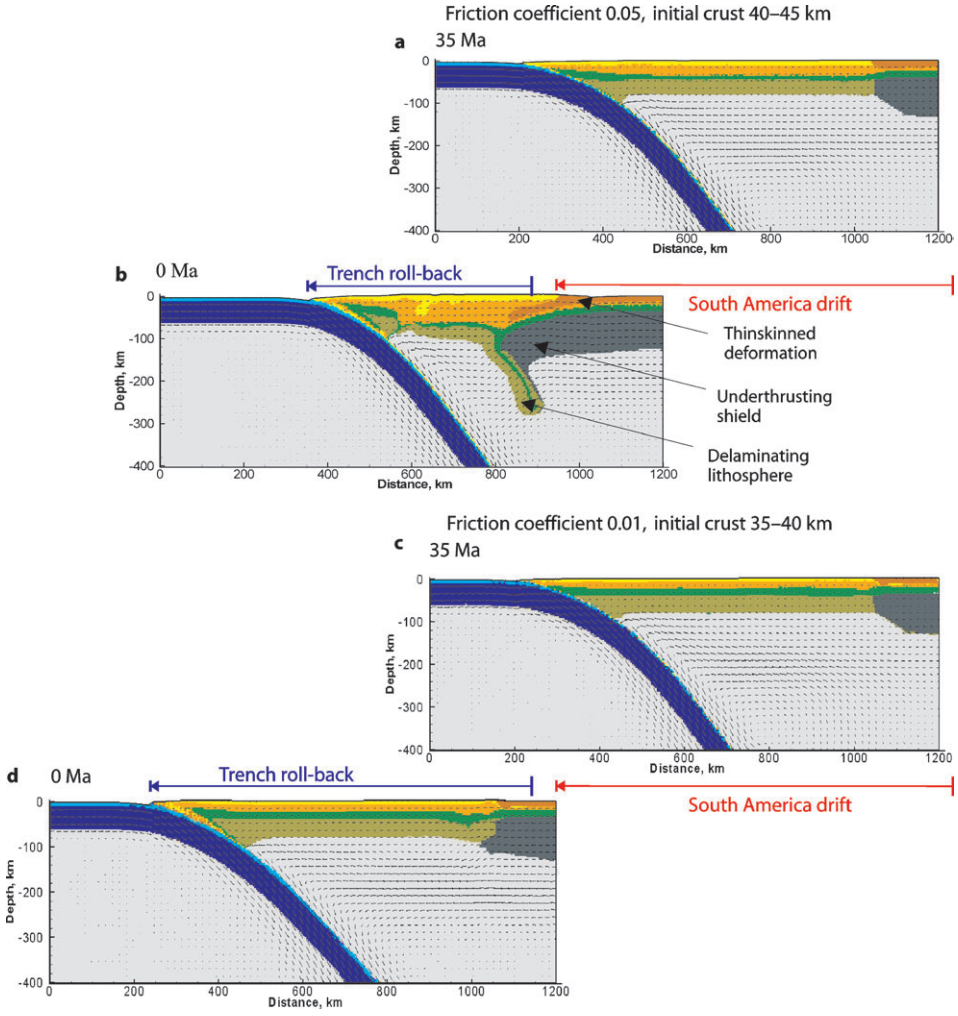

Fig. 25.4.
Time snapshots of the evolution of tectonic shortening for the models of the Central Andes (**a, b**) and Southern Andes (**c, d**). Color codes correspond to rock types. In the Central Andes' model, about 60% of the South American westward drift is accommodated by trench roll-back and about 40% by tectonic shortening at the South American margin. Note the intensive thickening of the felsic upper crust (*yellow*, *orange*) and the loss of mafic lower crust (*green*) in the South American Plate in the Central Andes. Note, also, that mantle lithosphere (*light green*) in the South American Plate in the Central Andes becomes thinner during tectonic shortening. At about 10 Ma, the sedimentary cover of the shield margin (*red*) fails and the shield begins to underthrust the growing plateau. In the Southern Andes' model, 95% of the South American westward drift is accommodated by trench roll-back and the South American Plate remains largely undeformed

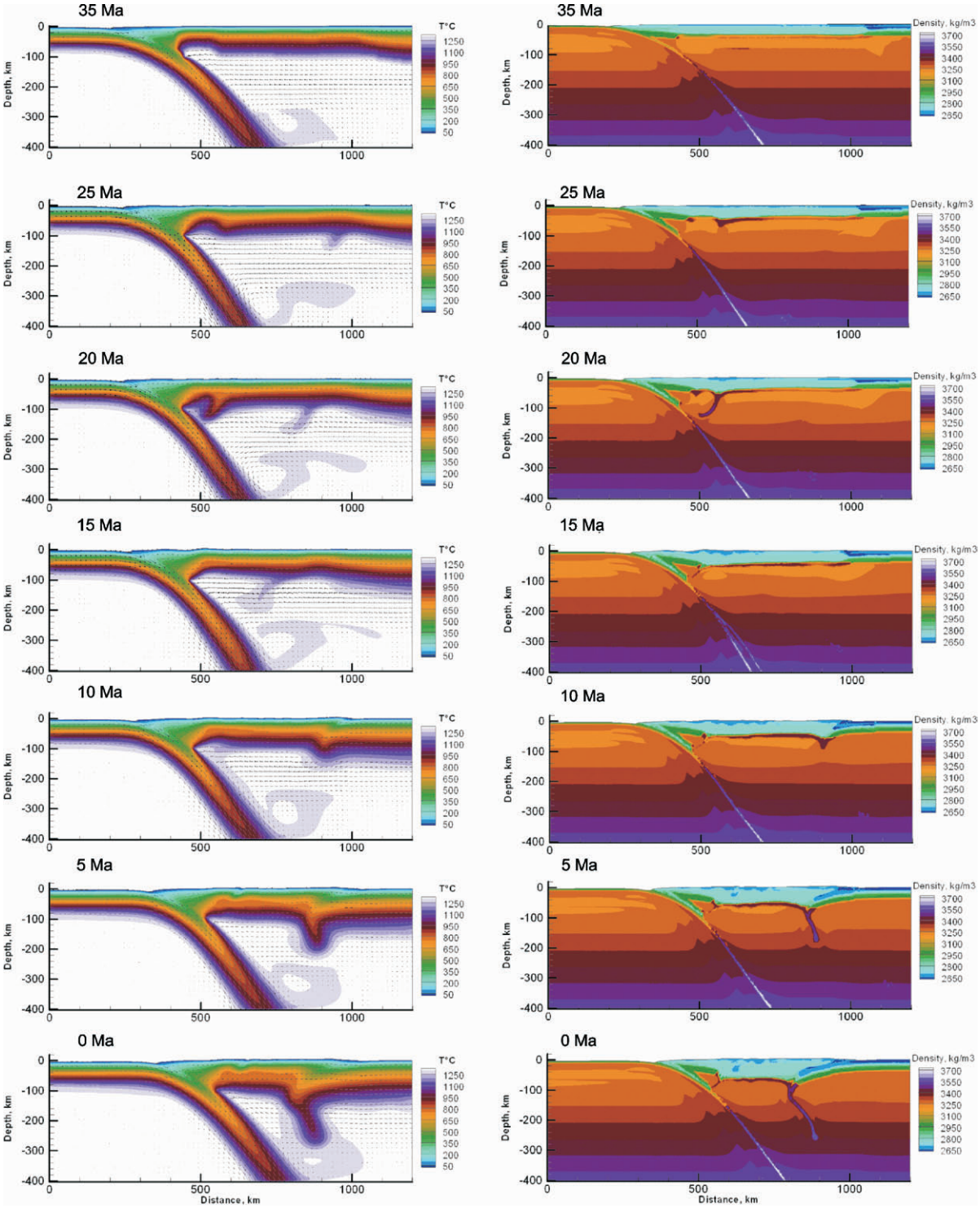

Fig. 25.5. Time snapshots of the evolution of temperature (*left*) and density (*right*) for the Central Andes' model

While sinking, most of these bodies are moved by corner flow towards the trench, join the slab and are then subducted into the mantle (Fig. 25.5, see also animations 2, 3 and 4 on the Supplementary DVD).

The model shows at 10 Ma that tectonic shortening generated high topography near the magmatic arc and in the back-arc close to the shield margin (Fig. 25.6, orange curve). These large topographic gradients initiated inten-

sive flow in the lower and middle crust. They also evened out crustal thickness and surface topography and produced a 4 km-high plateau during the last 5–10 million years (Fig. 25.6). At the same time, tectonic shortening reached 350 km, in agreement with the geological estimations of the maximum shortening in the Central Andes (Kley and Monaldi 1998).

The model also predicts failure of the foreland sediments at about 10 Ma followed by underthrusting of the shield margin and a switch from a pure-shear to a simple-shear mode of shortening. This concurs with both the geological model by Allmendinger and Gubbels (1996) and the back-arc-focused numerical study by Babeyko and Sobolev (2005). Figure 25.7 demonstrates the evolution of tectonic deformation, showing calculated, finite-strain distribution at 18 Ma and 0 Ma. At 18 Ma, deformation is moderate and it is dominated by pure shear. In contrast, the final stage of deformation is dominated by simple shear, which is accommodated by underthrusting of the shield margin and lower-crustal flow beneath the plateau.

During tectonic shortening, the temperature of the crust markedly changes (Fig. 25.5). The delamination of the lower crust and mantle lithosphere results in strong heat input into the crust, which leads to partial melting and then convection within the thick, felsic crust (Babeyko et al. 2002). As the resolution of the current model was too low to reproduce small-scale convection in the crust, we emulated such convection by increasing the heat conductivity of the felsic material by ten times if its temperature exceeded 750 °C. The result of this process is a zone of high temperature (higher than 750 °C) rapidly growing in the thickened crust (Fig. 25.5, see also animation 3 at Supplementary DVD) in accordance with present-day high heat flow in the Altiplano (Springer and Förster 1998).

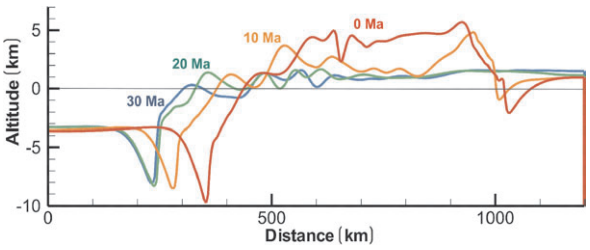

Fig. 25.6. Evolution of surface topography in the Central Andes' model. Note the formation of high topography followed by a plateau growth during the last 10 Myr

25.3.2 Sensitivity of Tectonic Shortening

Here we examine the sensitivity of tectonic shortening to potentially important factors such as the overriding rate, the strength of mechanical coupling between the subducting and overriding plates, the initial lithospheric structure, and the convergence rate. To do that, we modified the Central Andes' model described above by "switching off" different factors and examining the consequences for tectonic shortening over the last 35 million years of evolution.

The shortening curve corresponding to the Central Andes' model is shown in Fig. 25.8b by black solid circles. Firstly, we "switched off" the acceleration of the South American westward drift in the Central Andes' model (e.g., drift velocity remained 2 cm yr^{-1} instead of increasing from 2 to 3 cm yr^{-1}), leaving all other parameters unchanged. This modified model (curve denoted by open boxes in Fig. 25.8b) generated only about 60% of the shortening achieved in the original Central Andes' model. Moreover, if the drift velocity was decreased to 1 cm yr^{-1},

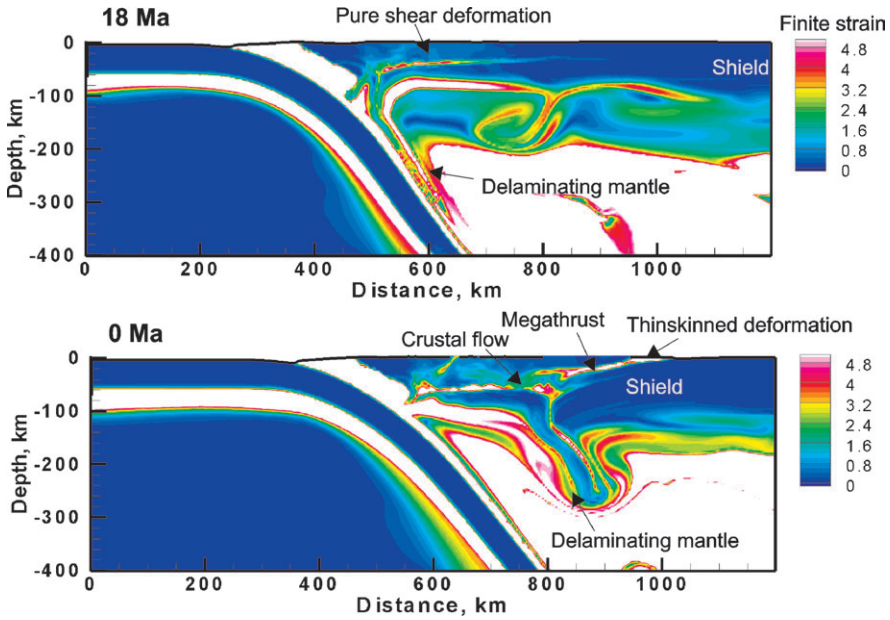

Fig. 25.7. Calculated finite strain in the Central Andes' model at 18 Ma and 0 Ma. Note the clear signatures of mega-thrust, thin-skinned deformation in the foreland, lower crustal flow, underthrusting of the shield margin and delamination of mantle lithosphere

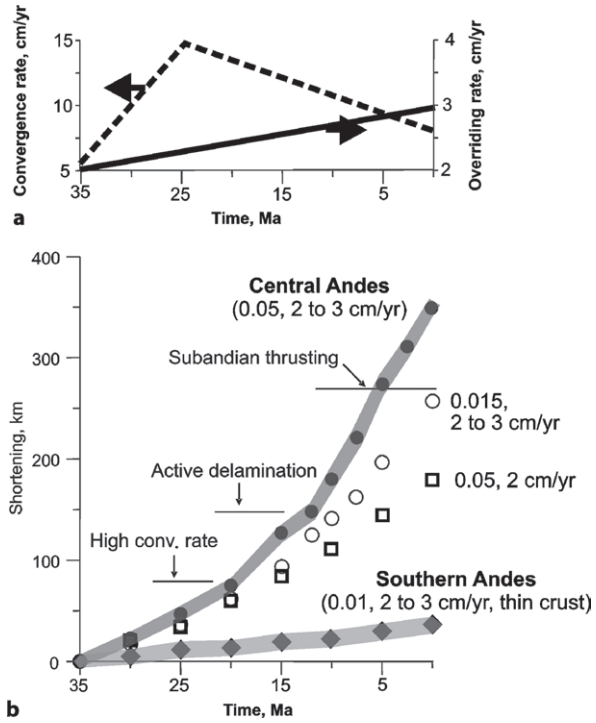

Fig. 25.8. **a** Variation over time in the convergence rate and overriding rate implemented in the model through boundary conditions; **b** Resulting tectonic shortening versus time for different models. *Numbers* near the models indicate the subduction-channel friction coefficient (*first number*) and the South American westward drift velocity (*second group of numbers*). Also shown are the time ranges of some critical processes in the Central Andes' model

there was no tectonic shortening at all. This indicates that in the case of the low-angle subduction and relatively high subduction-channel friction which we consider here, the overriding velocity is among major factors effecting deformation of the overriding plate.

Next, we "switched off" the relatively high, subduction-channel friction in the Central Andes' model by setting μ to 0.015 instead of 0.05. The resulting model (Fig. 25.8, curve indicated by open circles) still generated a large amount of tectonic shortening, i.e. 74% of the shortening achieved in the original model. This model shows that large changes in the friction coefficient (by three to four times) alone do not lead to dramatic changes in the rate of tectonic shortening. Now, if in addition to the change in the friction coefficient, we adopt a thin-crust (35–40 km) initial model instead of a thick-crust (40–45 km) model, then the tectonic shortening at 0 Ma is reduced to less than 40 km (Fig. 25.8b, filled diamonds). The reason for such behavior is discussed in the next section.

From the shape of the shortening curve for the Central Andes' model (Fig. 25.8b), it can be seen that the high convergence rate of 13–15 cm yr^{-1} achieved between 30 and 25 Ma had little effect on the shortening rate. This is a typical feature in all our models, demonstrating that large changes in the subduction rate (leading to large changes in the convergence rate) do not intesify shortening in the overriding plate.

In several numerical experiments, we changed the geometry of the subducting plate and kept all other parameters fixed. As expected, we observed an increase in the compression stress in the overriding plate when the subduction angle decreased (flatter subduction). Although these effects clearly deserve a more systematic investigation, it is clear that at low interplate friction (coefficient about 0.01), relatively small changes in the subduction angle can result in changes to the stress field of the overriding plate from slight compression to slight tension.

In addition to the factors considered above, some other processes can also influence the rate of tectonic shortening. As previously discussed, the clear increase in the shortening rate in the Central Andes' model at about 10 Ma (Fig. 25.8b) is associated with the failure of the foreland sediments followed by underthrusting of the shield margin and a switch from a pure-shear to a simple-shear mode of shortening. Another important process leading to the weakening of the upper plate, and also to a periodic change in the strength of viscous coupling between the upper and lower plates, is delamination of the lower crust and mantle lithosphere of the upper plate, which we discuss in the following section.

25.3.3 Consequences of Mantle Delamination

Before delamination takes place, mineral reactions result in a density increase in the thickening, lower, mafic crust of the overriding plate (Fig. 25.5). The consequence is that little surface uplift occurs despite the increasing thick-

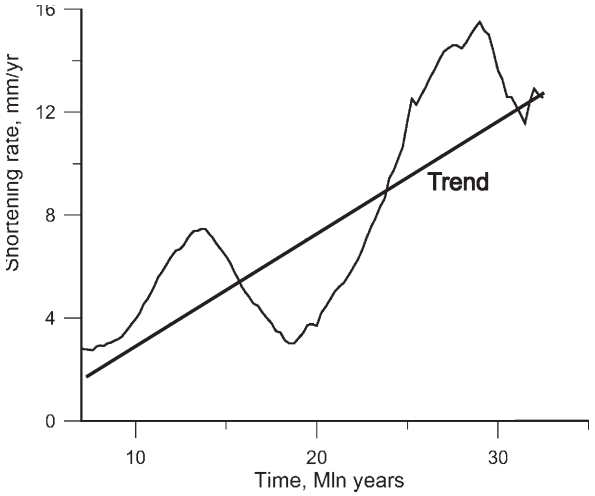

Fig. 25.9. Variation in the shortening rate with time in one version of the Central Andes' model. The general tendency for increased shortening is due to the rising rate of the South American westward drift. The reason for periodic variation is explained in Fig. 25.10

ness of the crust (see Fig. 25.6, blue and green curves corresponding to the model time of 30 and 20 Ma respectively). This, in turn, makes tectonic shortening energetically very efficient because no mechanical work is spent against gravitational spreading of the rising surface topography. (For more discussion concerning this process see Babeyko et al. 2006, Chap. 24 of this volume).

To look at the effect of mantle delamination in more detail, we considered a modification of the Central Andes' model, which has a slightly different distribution of initial crustal thickness than the model discussed above. This modified model shows basically the same features as the Central Andes' model presented below, but delamination and related processes are more pronounced in this particular model. Figure 25.9 shows the evolution of the tectonic shortening rate computed for this particular model which has two prominent peaks at ~13 and 29 Ma.

The origin of the first peak is illustrated by Fig. 25.10 (see also animation 7 at Supplementary DVD), which shows a sequence of snapshots of the modeled thermal

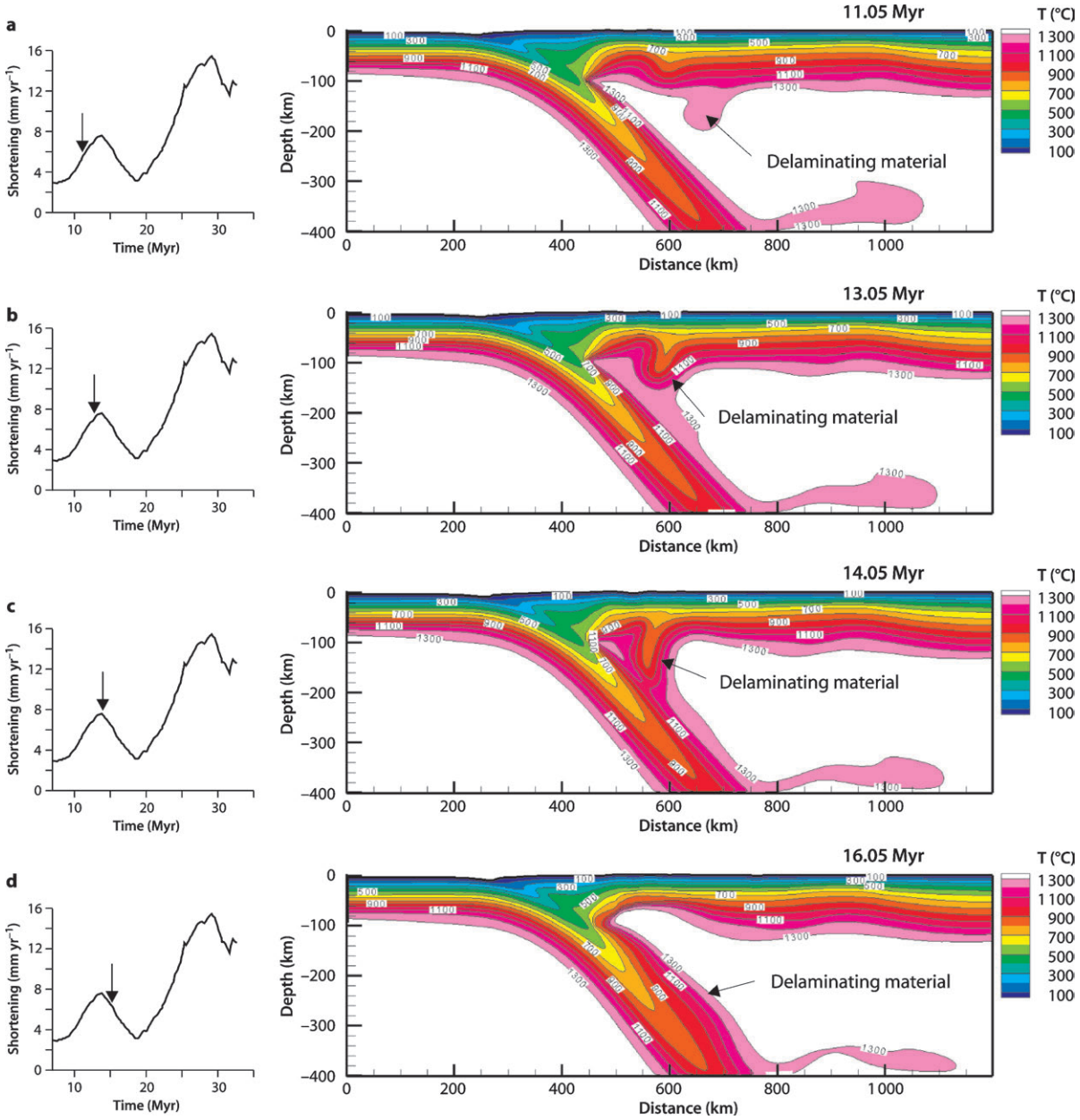

Fig. 25.10. Time snapshots of the temperature distribution in a version of the Central Andes' model (*right column*). The *left column* of figures shows the shortening-rate with *arrows* indicating the time of the corresponding temperature snapshots. Note that the maximum shortening rate corresponds to the blocking of the asthenospheric wedge by delaminating mantle material

structure. It is seen that when the tip of the corner flow is occupied by hot asthenospheric material (white), the shortening rate of the upper plate is relatively low. However, when delaminated mantle material, moving by corner flow, blocks its tip, the shortening rate of the upper plate is at a maximum. This behavior is caused by increased viscous coupling between the plates when the asthenospheric wedge is blocked by the cool, delaminated mantle material. Increased mechanical coupling increases the upper plate's resistance to overriding, which intensifies its deformation.

Another important consequence of mantle delamination is heating of the crust. Figure 25.10d shows that after the delaminated material is transported down by the slab, the hot asthenosphere (*white*) rises almost to the level of the Moho. This creates a strong heating impulse that partially melts the crust and may also trigger convection in the felsic crust (Babeyko et al. 2002). The mechanical consequence of this process is the weakening of the crust (Babeyko et al. 2006, Chap. 24 of this volume).

Overall, the consequence of mantle + lower-crust delamination and the preceding mineral reactions in the mafic lower crust of the overriding plate is a significant increase in the susceptibility of the upper plate to tectonic shortening. This result leads to an important conclusion about the possible evolution of tectonic shortening in the upper plate: Because mantle delamination is driven by gabbro-eclogite transformation and the latter occurs only when crustal thickness exceeds some 45 km, the shortening rate may be expected to be relatively low before the crust of the upper plate reaches this critical thickness. After the critical thickness is achieved, the shortening rate increases.

25.4 Addressing Key Questions of the Andean Orogeny

25.4.1 Why Has the High Plateau Developed Only during the Last 30 Million Years?

There are many arguments for the idea that the most important condition for creating the Altiplano-Puma Plateau was crustal thickening caused by extensive tectonic shortening that occurred in the Central Andes during the Cenozoic (Isacks 1988; Allmendinger and Gubbels 1996, Allmendinger et al. 1997; Lamb et al. 1997; Kley and Monaldi 1998; Giese et al. 1999). Therefore, the question about plateau formation is subdivided: (*1*) Why has the extensive tectonic shortening occurred only during the last 30 million years? and (*2*) How has tectonic shortening created the high plateau?

As shown in the previous section, a modeled increase in convergence rate from 6 to about 15 cm yr^{-1} did not change the shortening rate of the overriding plate significantly (see Fig. 25.8). Moreover, our modeling shows no correlation between the shortening and convergence rates (compare Fig. 25.8a,b). This concurs with data for the Central Andes, which also lacks such a correlation (Oncken et al. 2006, Chap. 1 of this volume), and for subduction zones in general (Heuret and Lallemand 2005). An increase in subduction rate does not lead to upper plate shortening because subduction driven by slab pull induced by slab negative buoyancy always leads to trench roll-back (Christensen 1996). If the subduction rate increases the trench roll-back rate should also increase, resulting in extension, rather than compression of the overriding plate. From this, we infer that it is unlikely that an increased convergence rate caused by the faster subduction of the Nazca Plate could have led to the intensive orogeny in the Central Andes.

It is argued (Lamb and Davis 2003) that another possible cause of the Cenozoic tectonic shortening is late Cenozoic aridization of the global climate, which resulted in reduced sedimentary fill in the trench that, in turn, led to an increase in interplate coupling. This idea looks attractive at first glance because it is consistent with two independent and remarkable correlations: (*1*) the temporal correlation between global ocean temperature and the shortening rate in the Central Andes during the last 25 million years (Lamb and Davis 2003; Oncken et al. 2006, Chap. 1 of this volume) and (*2*) the spatial correlation between the magnitude of tectonic shortening and the thickness of the sedimentary trench-fill off the south-Central Andes (Lamb and Davis 2003; see also Fig. 25.1). Oncken at al. (2006, Chap. 1 of this volume) discuss the Lamb and Davis (2003) hypothesis from a geological viewpoint, whereas we discuss it here based on the results of our modeling.

As seen in the previous section, a three- to fourfold change in the interplate (subduction-channel) friction coefficient at constant other model parameters, may result in a change in the magnitude of tectonic shortening by about 30% (~100 km) in the Central Andes (see Fig. 25.8b). This result shows that if a climate-controlled increase in the subduction-channel friction coefficient were of the order of five times or more, then climate would indeed be an important control on the tectonic shortening rate.

According to the geological data (Oncken et al. 2006, Chap. 1 of this volume), the average thickness of the sedimentary trench-fill was less than 0.5 km off the Central Andes between 30 and 50 Ma, and less than 0.2 km since 30 Ma. Our calibration of the relationship between subduction-channel friction and the thickness of the trench-fill (Fig. 25.12, see Sect. 25.5.1 for explanation) translates the above values into interplate friction coefficients of 0.03–0.05 between 30 and 50 Ma and close to 0.05 since 30 Ma. According to our modeling results, such small changes in the friction coefficient (by 1.6 or less) cannot significantly

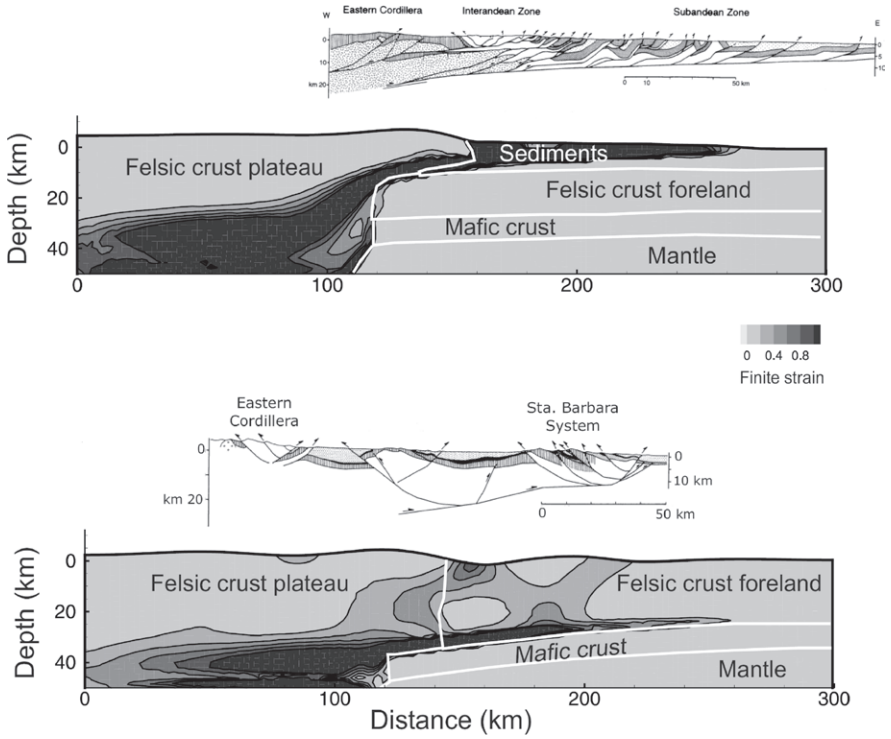

Fig. 25.11.
Models and observations for two cross sections in the Central Andes: (**a**) the Altiplano and (**b**) the Puna. Geological sections are from Kley et al. (1999) and modeling results from Babeyko and Sobolev (2005). *Gray colors* in the model cross sections indicate the magnitude of the cumulative, finite-strain norm (square root of the second invariant of the strain tensor). Note the significant difference in the deformation styles between the Altiplano and Puna segments, and the good correspondence between the models and the geological data

change the tectonic shortening rate. From this, we conclude that it is unlikely that climate was the primary reason for the increased rate of tectonic shortening in the Central Andes during the Cenozoic, as suggested by Lamb and Davis (2003). However, although our modeling does not support this part of the Lamb and Davis (2003) hypothesis, we agree with these authors that the large difference in interplate friction between the Central Andes and rest of the Andes might have contributed to the different magnitudes of tectonic shortening in these regions.

Of all the factors considered in our models, tectonic shortening appears to be the most sensitive to the overriding rate of the upper plate (Fig. 25.8). With a low overriding rate of 1 cm yr^{-1} or less, and other parameters fixed, we did not observe any shortening. With a constant overriding rate of 2 cm yr^{-1}, the shortening reached 180 km at 0 Ma and when the overriding rate increased from 2 to 3 cm yr^{-1}, the tectonic shortening reached 350 km. These results strongly suggest that the late Cenozoic acceleration of the westward drift of the South American Plate might have been a primary cause of the Central Andean orogeny, in agreement with the earlier proposal of Russo and Silver (1994). This also concurs with the observed correlation between the overriding velocity of South America and the shortening rate in the Central Andes (Oncken et al. 2006, Chap. 1 of this volume), and with such correlations for subduction zones in general (Heuret and Lallemand 2005).

Our models show that large amounts (over 300 km) of tectonic shortening that are accompanied by delamination of the mantle lithosphere and mafic lower crust, always generate a high plateau. The exclusion from this rule may be those cases where an exceptionally large erosion rate exists (Babeyko et al. 2006, Chap. 24 of this volume). This does not apply, however, to the Central Andes. One reason that large amounts of tectonic shortening generates high plateau is that the weak, felsic, middle-lower crust cannot maintain the high stresses associated with the large gradients in surface topography created by the tectonic shortening. The consequence is middle-lower crustal flow that tends to flatten the Moho and surface topography, which has also been demonstrated in earlier models (e.g., Royden 1997, Husson and Sempere 2003). Additionally, the basins-and-ranges structure created by the buckling of the shortened lithosphere is smoothed by internal erosion and drainage, which also contributes to the formation of the plateau-like surface topography.

25.4.2 Why Are the Central and Southern Andes so Different?

While the high and increasing overriding rate of the South American Plate during the last 30 million years can explain the most extensive tectonic shortening over that time, it does not explain the large amounts of shortening in the Central Andes and the small amounts in the Southern Andes. Russo and Silver (1994), suggested that South America's trenchward motion is driven by deep mantle

flow coupled to its base which "collides" with the Nazca Plate; the stagnation point and maximum compression stress occur in the Central Andes. However, in this model it remains unclear how the stresses would differ (if at all) between in the center and periphery of the South American leading edge. Moreover, recent seismic data (Helffrich et al. 2002) argue against the mantle flow pattern predicted by the Russo-Silver model (Russo and Silver 1994). We do not think that these arguments allow a rejection of the mantle-flow model by Russo and Silver (1994), but they indicate the possibility of alternatives.

Leaving this decision for further three-dimensional numerical analysis, we suggest here another explanation for the concentration of deformation in the Central Andes. We note two important differences in the crustal structure of the central and Southern Andes. Firstly, the thickness of the sedimentary fill in the trench off the Southern Andes is more than 1.5 km, whereas it is less than 0.5 km off the Central Andes (see Fig. 25.1), and a similar situation could be expected for the entire Cenozoic (Oncken et al. 2006, Chap. 1 of this volume). According to our model (see Sect. 25.5.1), this corresponds to an interplate friction coefficient that is three to five times lower in the Southern Andes than in the Central Andes. Secondly, in the Southern Andes, the thickness of the crust is, even now, less than 40 km and it has a relatively thick, mafic, lower part (Lüth and Wigger 2003; Tassara 2004). In the Central Andes, however, the crust is likely to have already significantly thickened (probably to more than 40–45 km) by 35 Ma (Lamb et al. 1997), and even at that time it might have been rather felsic (Lucassen et al. 2001; Tassara 2004).

The numerical model that lowers the interplate friction coefficient by five times in the Southern Andes and also uses a thinner crust there, compared to the Central Andes at 35 Ma, generates less than 40 km of tectonic shortening at the present time, even with a high, and increasing, overriding rate for the South American Plate (Fig. 25.8b). In this model, most of the South American Plate's drift is accommodated by roll-back of the Nazca Plate (Figs. 25.4c,d). As a result, the South American Plate overrides the Nazca Plate more than 300 km further in the Southern Andes' model (Fig. 25.4d) than in the Central Andes' model (Fig. 25.4b).

Another explanation for the difference between the central and Southern Andes was suggested by Yanez and Cembrano (2004). These authors proposed that the younger age of the subducting Nazca Plate in the Southern Andes results in regionally lower, shear coupling between the plates, which, in turn, leads to the smaller amount of deformation in the Southern Andes upper plate. Our modeling does not confirm this suggestion. If a subduction channel is introduced in the model, then shear coupling between the plates is controlled by the mechanical (mostly frictional) properties of the rocks within the channel rather than by the age-dependent temperature of the deeper part of the slab. Therefore, it may be expected that the presence or absence of a lubricant (trench sediment) is much more important in determining the magnitude of shear coupling between the plates than the age of the slab. This does not mean, however, that the slab age cannot affect deformation of the overriding plate. Such dependency might in fact exist is because trench roll-back also requires deformation (bending) of the subducting slab, which may well depend on slab age. Therefore, the trench could roll back more easily when the slab is younger, with consequently less deformation of the overriding plate.

25.4.3 Why Are the Altiplano and Puna Segments of the Central Andes Different?

We have run several numerical experiments focused on the deformation in the Andean back-arc (Babeyko and Sobolev 2005). In this model set-up, we prescribed the total magnitude of tectonic shortening with an eye to the factors that control deformation styles. We varied the temperature of the lithosphere and the strength of the sediments in the foreland. The finite strain distribution of two models replicates well the deformation patterns in the Altiplano (Fig. 25.11a) and Puna (Fig. 25.11b) segments of the Central Andes. Also shown are corresponding geological cross sections by Kley et al. (1999). The significantly different deformation styles result from the two segments differing in upper crustal strength (weak sediment in the Altiplano foreland and no such sediment in the Puna foreland) and lithospheric temperature (cold lithosphere in the Altiplano foreland and warm in the Puna foreland). For more details see Babeyko and Sobolev (2005).

Therefore, our modeling supports the idea of Allmendinger and Gubbels (1996) that the presence of thick Paleozoic sediment in the Altiplano foreland and the higher lithospheric temperature in the Puna foreland might have been the major cause of the different styles of tectonic shortening in these regions. To accomplish this, the sediments had to become very weak (their effective friction angle must drop below 10°) at about 10 Ma. For discussion of the effects of the weakening lithosphere see Babeyko and Sobolev (2005) and Babeyko et al. (2006, Chap. 24 of this volume).

25.4.4 Which Scenario Is Most Plausible for the Andean Orogeny?

From our modeling, we infer the following scenario for the tectonic evolution of the Andes. The South American Plate has a long history of westward drift with its velocity

of 1–1.5 cm yr^{-1} increasing to 2–3 cm yr^{-1} during the last 30 million years (Silver et al. 1998). With these conditions, the dipping angle of the relatively young slab (younger than 50 million years in our case) decreases with time (von Hunen et al. 2004) increasing coupling of the slab with the overriding plate. Maximum coupling was achieved in the Central Andes, where the arid climate caused a lack of sediment in the trench (no lubrication), resulting in a relatively high, interplate friction coefficient of about 0.05 during the entire Cenozoic. With this high friction, the stress in the overriding plate became compressional when the overriding velocity exceeded 1–1.5 cm yr^{-1}. Therefore, the upper plate in the Central Andes was subjected to significant shortening at ~70 Ma (the Peruvian shortening phase) and in the late Cenozoic, beginning from some 50 Ma (Oncken et al. 2006, Chap. 1 of this volume). At the same time, in the Southern Andes, the upper plate was still under extension because of the lower interplate friction ($\mu \approx 0.01$) caused by the extensive inflow of lubricating sediment into the trench.

Long-term westward drift combined with high interplate friction in the Central Andes has resulted in ~200 km of continental crustal erosion since the Jurassic (Scheuber et al. 1994). Despite the upper plate in the Central Andes being under compression since ~50 Ma, its deformation rate was relatively low before ~30 Ma (Oncken et al. 2006, Chap. 1 of this volume). We suggest that there were two major reasons for this. Firstly, the crust was still relatively thin (< 45 km), which did not allow for eclogitization mineral reactions in the lower crust. In such a case, the mechanical work required to shorten the crust remains very high (Babeyko et al. 2006, Chap. 24 of this volume). Secondly, the overriding velocity was still too low to create the high compression needed for extensive deformation of the strong lithosphere.

At about 30 Ma, after the establishment of a "flat slab" in the Central Andes (Altiplano latitude) and after the associated episode of enhanced tectonic shortening (Isacks 1988), the crustal thickness in a large part of the Central Andes reached the threshold value (of about 45 km) when eclogitization reactions become activated. At this critical point, the lithosphere of the upper plate was effectively weakened (Babeyko et al. 2006, Chap. 24 of this volume) and continued to shorten extensively, even after the slab became steeper again at about 25 Ma (Isacks 1988).

At the same time, westward drift of the South American Plate had begun to accelerate, increasing compression and the rate of tectonic shortening in the upper plate. The tectonic shortening was concentrated in the Eastern and Western Cordilleras, where the lithosphere was relatively weaker and where the crustal thickness first reached the threshold value of 45 km. Continuing tectonic shortening, accompanied by the eclogitization of the thickening lower crust, triggered delamination of the lower crust and mantle lithosphere. The delamination was followed by the thickening, heating, and partial melting of the felsic part of the crust (Babeyko et al. 2002). Finally, the ductile flow in the heated, and weak, felsic crust evened out the Moho and surface topography and created the high plateau in the Central Andes.

The above scenario applies to the Altiplano segment of the Central Andes. Tectonic evolution of the Puna segment was different most likely because of the following factors: (*1*) the flat slab episode in the Puna occurred some 10 to 20 million years later (Kay et al. 1999), so the crust only reached the critical thickness of 45 km at about 10–15 Ma; (*2*) the higher temperature in the foreland lithosphere in the Puna allowed thick-skinned tectonic shortening in the foreland; and (*3*) the absence of thick and weak Paleozoic sediment in the Puna foreland prevented thin-skinned deformation. As a result, tectonic shortening in the Puna and its foreland was not as intensive and occurred later than that at the latitude of the Altiplano. The consequence was a sig-nificantly smaller magnitude of the total shortening (Kley and Monaldi 1998) and a more recent episode of lower-crust + mantle-lithosphere delamination (Kay and Kay 1993).

The shortening rate in the Central Andes has generally tended to increase with time since about 50 Ma because of the increasing overriding velocity of the South American Plate. However, the shortening rate has varied owing to several processes that led either to the weakening of the upper plate (such as failure of the foreland sediment) or an increase in interplate coupling caused by, for example, delaminating mantle material blocking corner flow.

In contrast to the Central Andes, in the Southern Andes, the high overriding rate of the South American Plate was almost entirely accommodated by the roll-back of the Nazca Plate. This was possible because of the combined effect of low friction in the well-lubricated (by sediment) subduction channel and the relatively strong lithosphere with a thin (< 40 km) crust. The upper plate was in a low-stress regime during the entire Cenozoic. Changes in the stress field from little extension to small amounts of compression in the Southern Andes (Vietor and Echtler 2006, Chap. 18 of this volume) might have been caused by the increasing overriding rate of the South American Plate and by changes in the geometry of the subducting plate, with the latter probably related to the concurrent processes in the Central Andes.

Finally, the combined effect of the different, late Cenozoic, trench roll-back distances (> 300 km difference) and the amount of Cenozoic, upper-plate erosion (about 200 km difference) in the central and Southern Andes is the spectacular Bolivian orocline. This orocline, according to our model, marks the region of maximum mechanical coupling between the plates during the last 100 million years.

25.4.5 Why Do Andean Surface Topography and Slab Geometry Correlate?

Although the Nazca slab dips at rather low angle everywhere beneath the South American Plate, there are significant north-south variations (Isacks 1988; Gephart 1994). Interestingly, the slab is steepest beneath the highest surface topography in the Central Andes, and it is less steep, or even flat, beneath the lower Southern and Northern Andes (Gephart 1994). This correlation is counter-intuitive because the strongest coupling between the plates, and the most deformation in the upper plate, could be expected to occur at a shallow dipping angle and, therefore, has a large coupling interface with the upper plate. Gephard (1994) suggested that the observed correlation indicates that slab geometry controls deformation of the upper plate. However, based on our modeling results, we suggest that the situation may, in fact, be vice versa, i.e. that the deformation of the upper plate may significantly influence the slab geometry.

The results of numerical models for the central and Southern Andes show the importance of upper-plate crustal structure and the interplate friction. The boundary conditions (e.g., slab pull rate and South American-plate push rate) and the initial geometry of the slab are exactly the same in both models. After 35 million years of evolution, the slab in the Central Andes' model became steeper (Fig. 25.4a,b), while in the Southern Andes' model, the slab became less steep (Fig. 25.4c,d). The present-day slab beneath the strongly shortened crust of the high Central Andes (Fig. 25.4b) is dipping at significantly larger angle than beneath the much less deformed crust of the low Southern Andes (Fig. 25.4d).

This is because the geometry of the subducted plate is largely controlled by the rate of trench roll-back (e.g., von Hunen et al. 2004); the higher the roll-back velocity, the less steeper the plate becomes. In the Southern Andes' model, almost the entire rate of upper-plate westward drift was accommodated by trench roll-back, and therefore the plate became less steep with time. In the Central Andes, a large part of the drift rate was accommodated by the shortening of the upper plate and, therefore, the rate of trench roll-back was lower than in the Southern Andes' model, with the consequence of a more steeply dipping slab. Moreover, as suggested by the numerical model of von Hunen et al. (2004) it is much easier to create a "flat slab" regime for a fast trench roll-back, than for a slow trench roll-back. This may explain the appearance of flat slab segments in the Southern and Northern Andes.

25.5 Deriving and Testing Model Predictions

A number of testable predictions can be derived from the model of the Andean orogeny described above. We discuss these predictions below.

25.5.1 Magnitude and Along-Strike Variation in Interplate Friction

Our modeling suggests that the friction coefficient in the subduction channel must be lower than 0.1 to allow the subduction zone to survive. Moreover, the friction should be even lower to fit the observed magnitudes of tectonic shortening in the Central Andes ($\mu \approx 0.05$) and Southern Andes ($\mu \approx 0.01$). These values are in good agreement with estimates of the subduction zone's friction coefficients based on geothermal constraints (Tichelaar and Ruff 1993, Peacock 1996). However, they are well below the lowest friction coefficients measured for rocks in laboratory experiments (0.1–0.15 for clay minerals according to Kopf and Brown 2003). This means that additional factors decrease the friction coefficient, such as hydrostatic fluid overpressure in the subduction channel rocks.

As discussed above, our modeling suggests that the completely different styles of tectonic evolution during the last 30 million years in the central and Southern Andes could have resulted because the Central Andes had both a ~5–10 km-thicker crust at 35 Ma and a higher (by 3–5 times) friction coefficient in the subduction channel compared to the Southern Andes. The regionally greater thickness of the crust in the Central Andean back-arc at 35 Ma was likely the cumulative result of a long history of tectonic shortening, enhanced during a "flat slab" episode (Isacks 1988) that was absent in the Southern Andes. The difference in subduction-channel friction between the two regions may reflect climate-controlled variations in the supply of sediment fill to the trench (Lamb and Davis 2003). However, the question arises as to whether there is any independent evidence for a variation (by several times) in trench friction between the central and Southern Andes.

One prediction of our model is that the down-dip limit of the frictional (brittle) domain of the subduction channel in the Southern Andes is significantly deeper than in the Central Andes, caused by the difference in the model friction coefficients (see inlet in Fig. 25.2). With a friction coefficient of $\mu = 0.05$ in the Central Andes, our model predicts the brittle-ductile transition in the channel to occur at ~37–40 km depth, whereas at $\mu = 0.015$–0.01, this transition in the Southern Andes occurs at 55–60 km depth. Note, that while higher friction is applied to a narrower brittle zone in the Central Andes than in the Southern Andes, the total coupling (shear) force in the subduction zone still appears to be two to three times higher in the Central Andes.

Assuming that the stick-slip flow mechanism in the seismic coupling zone is related only to the frictional (brittle) rheology, we predict that the down-dip limit of the seismic slip zone (constrained by seismological data) as well as the down-dip limit of the locked zone (con-

strained by Geographical Positioning System = GPS data) should be significantly deeper in the southern than in the Central Andes. This model prediction agrees remarkably well with both seismological and GPS observations. Tichelaar and Ruff (1993) estimated the down-dip limit for the seismic coupling zone for large earthquakes to be 36–41 km in the Central Andes (north of the 28° S) and 48–53 km in the Southern Andes. At the same time, GPS observations by Khazaradze and Klotz (2003) and Klotz et al. (2006, Chap. 4 of this volume), completely independently of the seismological data of Tichelaar and Ruff (1993), infer maximum depths for mechanical coupling of about 33 km in the region north of 30° S and 50 km in the Southern Andes.

Using the GPS data (Khazaradze and Klotz 2003) and our modeling results, we can also try to estimate the variation in the interplate friction coefficient along the trench. From the definition of the depth to the brittle-ductile transition (see Eqs. 25.6 and 25.7 in Sect. 25.2.2) and assuming that the pressure and temperature change linearly with depth in the subduction channel, we obtain:

$$\mu \cdot H \approx \mathrm{C} \exp(-\gamma H) \tag{25.8}$$

where μ is the friction coefficient, H is the depth of the brittle-ductile transition in the subduction channel, and C and γ are constants. We can rewrite Eq. 25.8 in the form:

$$\frac{\mu}{\mu_0} \approx \frac{H}{H_0} \exp\left[\gamma(H - H_0)\right] \tag{25.9}$$

where index 0 denotes the reference value of the friction coefficient and the corresponding depth to the brittle-ductile transition. From our models, we estimate parameter γ to be 0.052. Using Eq. 25.9 and locking depths from the GPS data (Khazaradze and Klotz 2003), we estimate the ratio between friction coefficients in the central and Southern Andes to be about 4.5. This is remarkably close to the ratio of 3–5 which we obtained to explain the differences in the evolution of the central and Southern Andes over the geological timescale.

Now, we can estimate the relation between the subduction-channel friction coefficient and the thickness of the sedimentary fill in the trench (Fig. 25.12). On the ordinate, we show the friction coefficient calculated from Eq. 25.9 and GPS data on locking depths, assuming that the maximum friction coefficient equals 0.05. On the abscissa, we show the thickness of the trench sediment at the same latitudes as the GPS estimates of the locking depths according to Bevis et al. (1999). Despite the limited number of data points, Fig. 25.12 demonstrates systematic and logical changes in the friction coefficient with the sediment thickness saturated at about 1.5 km thickness. We interpret this behavior that the entire subduction channel is filled by sediment (lubricant) and further

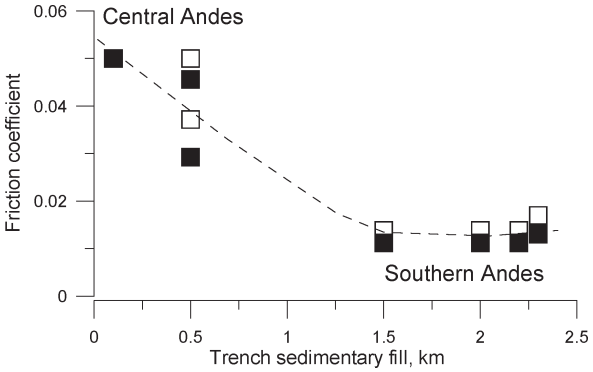

Fig. 25.12. Estimated interplate friction coefficient versus observed thickness of the sedimentary trench-fill between 20 and 40° S. *Open boxes*: It is assumed that the depth of the brittle-ductile transition corresponds to the bottom of the locked zone (see Khazaradze and Klotz 2003). *Solid boxes*: It is assumed that the depth of the brittle-ductile transition corresponds to the bottom of the transition zone (see Khazaradze and Klotz 2003). Note that the friction coefficient changes significantly with sedimentary thickness until the thickness reaches some 1–1.5 km; thicker than this, the friction coefficient reaches its asymptotical value of about 0.01

sedimentary addition does not change its friction properties, when the thickness of the trench sediment becomes higher than 1–1.5 km. Interestingly, this conclusion agrees with the observation of a global correlation between the thickness of trench fill and the transition from erosion- to accretion-type subduction (Clift and Vannucchi 2004).

25.5.2 Relationship between Arc Magmatism and Tectonic Shortening

Another model prediction follows from the comparison between the evolution of tectonic shortening and the evolution of the mantle temperature beneath the magmatic arc. As we have shown before (Fig. 25.10, see also animation 7 at Supplementary DVD), processing the delaminating material through the asthenospheric wedge by corner flow results in an increasing shortening rate. Simultaneously, the temperature of the asthenospheric wedge beneath the magmatic arc decreases, which must lead to reduced magmatic arc activity over the time period depending on the volume of the delaminating material (typically a few million years). This suggests an anti-correlation between the arc magmatic activity and tectonic shortening. Figure 25.13 shows a histogram of the magmatic activity in the Central Andes (Trumbull et al. 2006, Chap. 2 of this volume; Oncken et al. 2006, Chap. 1 of this volume) together with the rate of tectonic shortening (Oncken et al. 2006, Chap. 1 of this volume). Although the estimation of magmatic activity is still rather controversial (Trumbull et at. 2006, Chap. 2 of this volume), there is, indeed, indication of the anti-correlation between arc magmatic activity and shortening rate.

Our model also predicts strong heating of the overriding-plate crust some 5–10 million years after a large volume of delaminated material was processed through the asthenospheric wedge by corner flow (Fig. 25.5, see also animations 3 and 7 at Supplementary DVD). This may result in the ignimbrite volcanism 5–10 million years after a peak of arc activity, the latter associated with the input of hot asthenospheric material in the wedge just after delamination (Fig. 25.5, see also animations 3 and 7 at Supplementary DVD). The peak of ignimbrite activity in the Central Andes at 8 Ma has indeed followed about 7 million years after the large peak of magmatic arc activity (Trumbull et al. 2006, Chap. 2 of this volume).

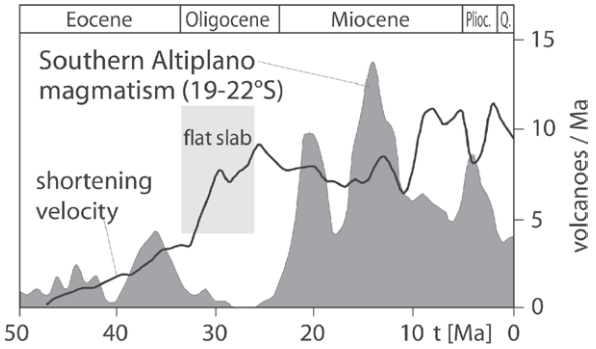

Fig. 25.13. Histogram of arc magmatic activity in the Central Andes (Trumbull et al. 2006, Chap. 2 of this volume; Oncken et al. 2006, Chap. 1 of this volume) together with the rate of tectonic shortening (Oncken et al. 2006, Chap. 1 of this volume). Note the tendency for anti-correlation between these two curves

25.5.3 Seismic Structure of the Crust and Upper Mantle

Here we compare the seismic tomographic images of the lithosphere-asthenosphere system of the Central Andes to expectations based on our modeling results. Figure 25.14 shows depth sections through the recent tomographic model by Koulakov et al. (2006). The tomographic images of P- and S-wave seismic velocities as well as the Q_p factor show similar features that are remarkably different in the crust and upper mantle as well as beneath the Altiplano and Puna Plateau. In the Altiplano (north of 23° S), the dominant low-velocity and high attenuation anomaly is located in the crust (see upper

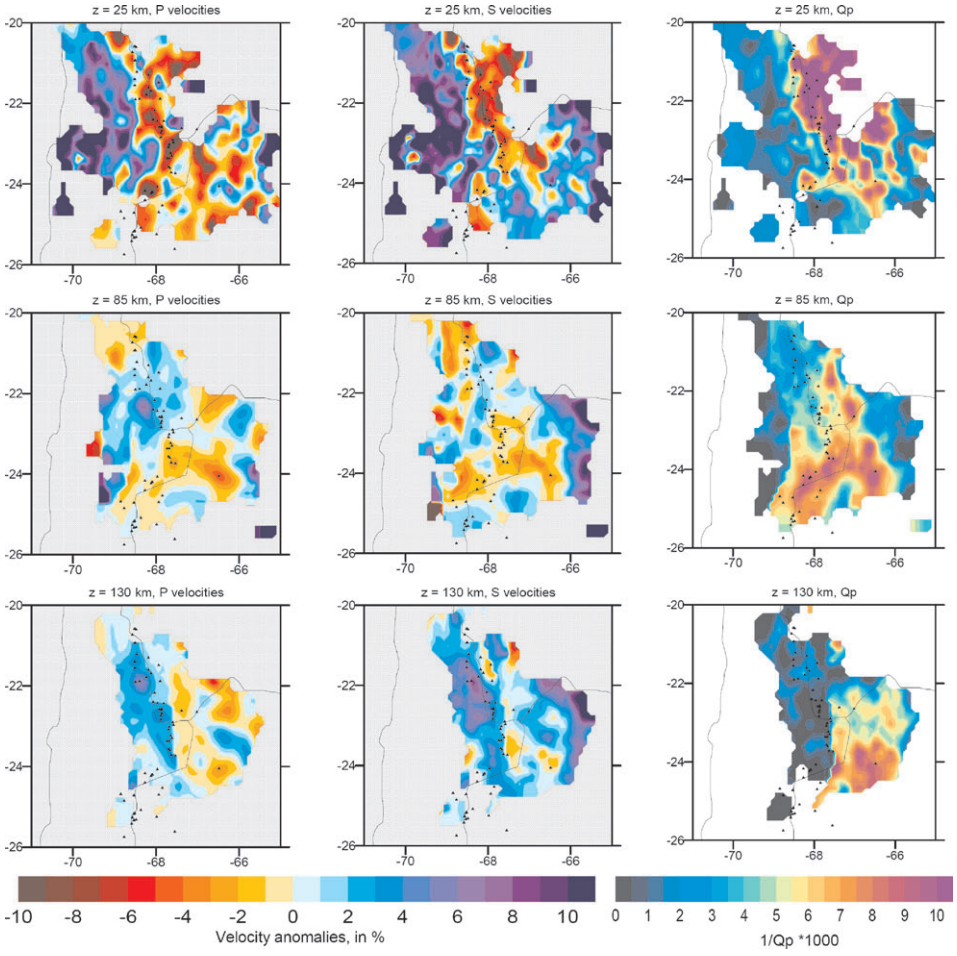

Fig. 25.14. Depth slices through the recent P- and S-wave and Q_p tomographic models of the Central Andes (Koulakov et al., in press). Note the significant change in the pattern from the crust to the upper mantle

row of images in Fig. 25.14), but in the Puna (south of 23° S), the dominant low-velocity anomaly is located in the mantle (see middle and lower row of images in Fig. 25.14).

This is an expected feature based on the tectonic history of these regions and our modeling results. In the Altiplano, tectonic shortening was already active for a few tens of millions of years (Allmendinger and Gubbels 1996, Oncken et al. 2006, Chap. 1 of this volume), which according to our model should have already resulted in delamination of the mantle lithosphere some 15 million years ago. The model predicts that the asthenospheric wedge should now be rather cool while the crust should be very hot (see Fig. 25.5, time snapshot at 0 Ma). In the Puna, most of the tectonic shortening was quite recent (Allmendinger and Gubbels 1996) and mantle delamination also happened recently (Kay and Kay 1993). In this case, the crust had no time to be heated, while the asthenospheric wedge should be occupied by hot, fresh, asthenospheric material that has recently replaced delaminated mantle (e.g., see Fig. 25.10d).

The high velocity and low attenuation anomaly in the mantle east of 67–68° W (see middle and lower sections in Fig. 25.14) probably represents the advancing margin of the Brazilian shield and is also clearly visible in all our geodynamic models. Figure 25.15 shows the results of direct, joint inversion of the P- and S-wave travel times and attenuation seismic data for temperature and water content in olivine of the mantle wedge at 23.5° S (Sobolev et al., in prep.). Estimated temperatures (Fig. 25.15a) are consistent with the advancing margin of the shield and with on-going delamination of the mantle lithosphere. The proxy for the water content in the mantle wedge, shown in Fig. 25.15b, is the pre-exponent factor in the relation for the seismic attenuation (Sobolev et al. 1996).

25.6 Looking beyond the Presented Models

The advanced numerical models presented in this paper are still limited and incomplete. Our 2D models ignore strike-parallel variations in structure, stress and velocity fields. One consequence is that the 3D focusing effect of the tectonic shortening (Hindle et al. 2005) is ignored. This means that the magnitude of tectonic shortening required for generating thick crust and high surface topography in the Central Andes is overestimated in our 2D models by up to 40% (Hindle et al. 2005). Our Central Andes' model requires 350 km of tectonic shortening since 35 Ma and some 100 km of shortening before that time. After correcting for the 3D focusing effect, we estimate the magnitude of the total tectonic shortening in the Central Andes to be about 320–350 km. This is close to the estimates by Oncken et al. (2006, Chap. 1 of this volume), but significantly less than estimates by McQuarrie and De Celles (2001).

Another consequence of our 2D approach is that we ignore the obliquity of subduction in the Andes. Because this obliquity was relatively small during the last 30 million years (Somoza 1998), its effect on major compression deformation is also likely to have been small. However, it may control strike-slip deformation in the Andes (Hoffmann-Rothe et al. 2006, Chap. 6 of this volume). A relatively straightforward way to consider the subduction obliquity is to apply an extended 2D modeling technique (Sobolev et al. 2005) that takes into account the 3D vector and tensor fields with no along-strike variation in structure and displacements, and therefore also enables the consideration of strike-slip deformation.

It is more difficult to account for any possible effects on trench roll-back and deformation of the upper plate caused by trench curvature and 3D flow in the mantle.

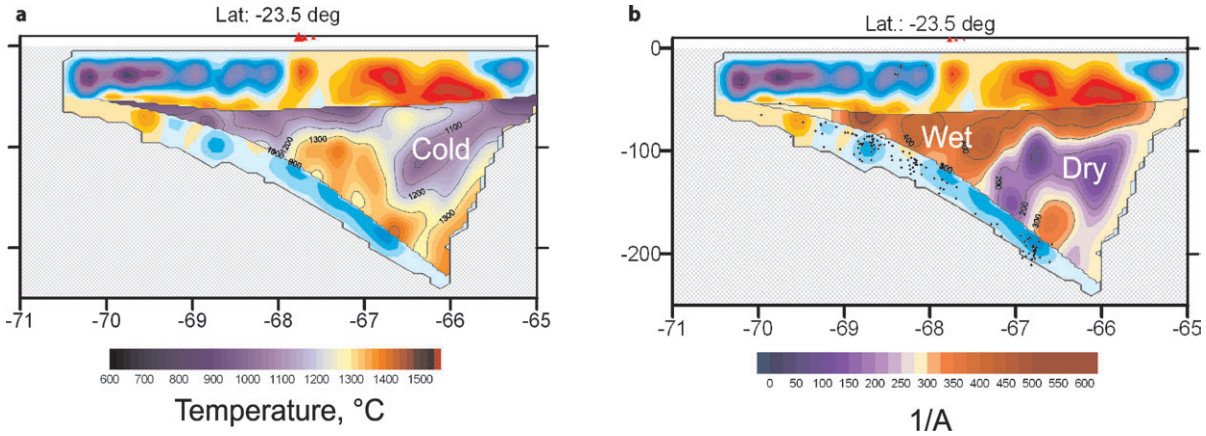

Fig. 25.15. Results of the direct inversion of the seismic data for temperature (**a**) and the inverse A factor (**b**) in the mantle wedge of the Central Andes (Sobolev et al., in preparation). The *colors* in the crust and in the slab show P-wave velocity variations in the tomographic model by Koulakov et al. (in press). The inverse A factor is a pre-exponent factor of the mineral physics relation for seismic attenuation as applied to olivine-dominated, ultramafic rocks (e.g., Sobolev et al. 1996), which is believed to be proportional to the water content of olivine

Thin-plate approximations, even extended to incorporate lower-crustal flow and interplate coupling (Medvedev et al. 2006, Chap. 23 of this volume), are not suitable for such a purpose. One possibility is a simplified 3D modeling technique that exploits the relatively slow variation in those parameters parallel to the strike of the Andes. Recently, this kind of technique was developed and employed for thermo-mechanical modeling of a pull-apart basin (Petrunin and Sobolev 2006).

As mentioned earlier in this chapter (Sect. 25.4.2), we cannot reject the possibility that the age of the Nazca slab has influenced trench roll-back mobility and, therefore, deformation in the overriding plate. This possibility can be tested with 2D models similar to the models presented in this paper. The reason we have not yet done this, is that, in addition to the slab age (temperature), the slab rigidity could also be affected by factors such as serpentinization (Ranero et al. 2003). Hydration can also significantly change rheology of the upper plate, not only switching from "dry" to "wet" peridotite rheology in the mantle lithosphere implemented in our model, but also through serpentinization of the fore-arc mantle (Gerya et al. 2002; Gerya and Yuen 2003).

In this work, we did not explicitly model the effect of a flat slab on deformation in the overriding plate, although we recognize its importance for the initial thickening of the crust to the critical thickness of 45 km. Partially, this kind of modeling can also be done using a 2D approach. However, our preliminary modeling results show that it is technically very difficult (if not impossible) to return from the flat-slab to the steep-slab configuration using 2D models (also mentioned by von Hunen et al. 2004), which limits the application of such modeling for the Andes.

Finally, what is still missing, is calculation of seismic velocities from the data on composition, temperature and pressure which all are available in our models, as recently presented by Gerya et al. (2006), but with full consideration of effects of anelasticity, water content and lattice preferred orientation on seismic velocities and seismic anisotropy. This is an interesting task for future studies.

25.7 Summary

We developed a coupled thermo-mechanical model of the interaction between subducting and overriding plates that employs realistic temperature- and stress-dependent, visco-elasto-plastic rheology and is focused on the late Cenozoic (last 35 million years) evolution of the Andes.

In the numerical experiments, we studied the conditions under which the overriding plate was tectonically shortened and we tested the sensitivity of shortening to several parameters including convergence rate, overriding rate, interplate friction and crustal structure of the upper plate. From this sensitivity study, we conclude that the major factor that controls tectonic shortening in the Andes is the fast and accelerating, westward drift of the South American Plate. However, we also infer that neither this drift nor any other factor was *alone* responsible for the orogeny in the Central Andes.

Our modeling suggests that the extreme orogeny in the Andes took place, at the time and in the location, when and where at least three major conditions were met: (*1*) a high overriding rate of the South American Plate; (*2*) thick crust (45 km) in the back-arc; and (*3*) a friction coefficient of about 0.05 in the subduction channel. The first condition was achieved over the last 30 million years and especially during the last 10 million years across the entire South American Plate. The second condition occurred only in the Central Andes due to tectonic shortening before 25–30 Ma, partially because shortening was enhanced during a "flat-slab" episode at about 30 Ma. The third condition was fulfilled also only in the Central Andes, where less than 0.5 km of trench sediment was accumulated owing to the arid climate. As a result, intensive tectonic shortening occurred only in the late Cenozoic and only in the Central Andes.

Our numerical models for the central and Southern Andes explain well the major features of Andean evolution during the last 35 million years. This includes the more than 300 km of tectonic shortening in the Central Andes accompanied by the underthrusting of the foreland and the formation of a 4 km-high plateau. Our models also explain the converse situation in the Southern Andes of less than 40 km of shortening and the absence of a high plateau. We show that the main reason for the difference in the late Cenozoic evolution of the central and Southern Andes could be the combined effect of the Southern Andes having a 5–10 km-thinner crust at 35 Ma and about five-times-lower interplate friction compared to the Central Andes. The result of the different magnitude of tectonic shortening and subduction erosion in the central and Southern Andes is the Bolivian orocline and a more steeply dipping subducting plate in the Central Andes than in the rest of Andes.

The models also demonstrate the important role of several processes that cause internal mechanical weakening of the South American Plate during tectonic shortening in the Central Andes. The main processes are gabbro-eclogite mineral reactions in the thickened, continental lower crust followed by lithospheric delamination, as well as the mechanical failure of the sediment covering the shield margin.

The modeling also suggests that the reason for the observed fluctuations in the shortening rate in the Central Andes may be increased viscous coupling between the plates caused when the asthenospheric wedge is blocked by the cool, delaminating, mantle material that is moving to the tip of the asthenospheric wedge by sub-

duction corner flow. Increased mechanical coupling increases resistance in the overriding of the upper plate which intensifies its deformation.

Several model predictions are consistent with observations. We show that the assumption of an interplate friction that is approximately five times smaller in the Southern Andes compared to the Central Andes is consistent with seismological and GPS data from the deeper seismogenic and locking zones of these respective regions. The model prediction of an anti-correlation between tectonic shortening and magmatic arc activity is also consistent with observations. And, finally, we have shown that our model predictions agree well with the known seismic structure of the crust and mantle in the Central Andes.

Acknowledgments

This paper is a contribution to the Deutsche Forschungsgemeinschaft project SFB-267 "Deformation Processes in the Andes". We thank members of the SFB-267 team for fruitful discussions and Ron Hackney and Allison Britt for useful comments and help in editing the manuscript. Tim Vietor is acknowledged for providing version of Fig. 25.1. Taras Gerya's thorough review helped to improve the paper. The Potsdam Institute of Climate has provided supercomputer facilities.

References

Allmendinger RW, Gubbels T (1996) Pure and simple shear plateau uplift, Altiplano-Puna, Argentina and Bolivia: Tectonophysics 259:1–13

Allmendinger RW, Jordan TE, Kay SM, Isacks BL (1997) The evolution of the Altiplano-Puna plateau of the Central Andes. Ann Rev Earth Planet Sci 25:139–174

Babeyko AY, Sobolev SV (2005) Quantifying different modes of the Late Cenozoic shortening in the Central Andes, Geology 33:621–624

Babeyko AY, Sobolev SV, Trumbull RB, Oncken O, Lavier LL (2002) Numerical models of crustal-scale convection and partial melting beneath the Altiplano-Puna plateau. Earth Planet Sci Lett 199:373–388

Babeyko AY, Sobolev SV, Vietor T, Oncken O, Trumbull RB (2006) Numerical study of weakening processes in the Central Andean backarc. In: Oncken O, Chong G, Franz G, Giese P, Götze H-J, Ramos VA, Strecker MR, Wigger P (eds) The Andes – active subduction orogeny. Frontiers in Earth Science Series, Vol 1. Springer-Verlag, Berlin Heidelberg New York, pp 495–512, this volume

Beck SL, Zandt G (2002) The nature of orogenic crust in the Central Andes. J Geophys Res 107: doi 10.1029/2000JB000124

Bevis M, Smalley R Jr, Herring T, Godoy J, Galban F (1999) Crustal motion north and south of the Arica deflection: Comparing recent geodetic results from the Central Andes. Geochem Geophys Geosyst 1: doi 1999GC000011

Bird P (1978) Stress and temperature in subduction zones: Tonga and Mariana. Geophys J R Astron Soc 55:411–434

Christensen UR (1996) The influence of trench migration on slab penetration into the lower mantle. Earth Planet Sci Lett 140(1–4): 27–39

Clift PD, Vannucchi P (2004) Controls on tectonic accretion versus erosion in subduction zones: implications for the origin and recycling of the continental crust. Rev Geophys 42: doi 10.1029/2003RG000127

Cundall PA, Board M (1988) A microcomputer program for modelling large-strain plasticity problems. In: Sowboda G (ed) 6th International Conference in Numerical Methods in Geomechanics, AA Balkema, Brookfield VT, pp 2101–2108

Gerya TV, Yuen DA (2003) Rayleigh-Taylor instabilities from hydration and melting propel 'cold plumes' at subduction zones. Earth Planet Sci Lett 212:47–62

Gerya TV, Stoeckhert B, Perchuk AL (2002) Exhumation of high-pressure metamorphic rocks in a subduction channel – a numerical simulation. Tectonics 6(21):1–19

Gerya TV, Connolly JAD, Yuen DA, Gorczyk W, Capel AM (2006) Seismic implications of mantle wedge plumes. Phys Earth Planet Int doi 10.1016/j.pepi.2006.02.005

Giese P, Scheuber E, Schilling F, Schmitz M, Wigger P (1999) Crustal thickening processes in the Central Andes and the different natures of the Moho-discontinuity. J S Am Earth Sci 12:201–220

Gleason GC, Tullis J (1995) A flow law for dislocation creep of quartz aggregates determined with the molten salt cell. Tectonophysics 247:1–23

Gregory-Wodzicki KM (2000) Uplift history of the Central and Northern Andes: a review. Geol Soc Am Bull 112:1091–1105

Hacker BR, Abers GA, Peacock SM (2003) Subduction factory 1. Theoretical mineralogy, density, seismic wave speeds, and H_2O content. J Geophys Res 108: doi 10.1029/2001JB001127

Handy MR, Wissing S, Streit SE (1999) Strength and structure of mylonite with combined frictional-viscous rheology and varied bimineralic composition. Tectonophysics 303:175–192

Hassani R, Jongmans D, Chery J (1997) Study of plate deformation and stress in subduction processes using two-dimensional numerical models. J Geophys Res 102:17951–17965

Heuret A, Lallemand S (2005) Plate motions, slab dynamics and backarc deformation. Phys Earth Planet Int 149:31–51

Hindle D, Kley J, Oncken O, Sobolev SV (2005) Crustal flux and crustal balance from shortening in the Central Andes. Earth Planet Sci Lett 230:113–124

Hirth G, Kohlstedt DL (1996) Water in the oceanic upper mantle: implications for rheology, melt extraction and the evolution of the lithosphere. Earth Planet Sci Lett 144:93–108

Hoffmann-Rothe A, Kukowski N, Dresen G, Echtler H, Oncken O, Klotz J, Scheuber E, Kellner A (2006) Oblique convergence along the Chilean margin: partitioning, margin-parallel faulting and force interaction at the plate interface. In: Oncken O, Chong G, Franz G, Giese P, Götze H-J, Ramos VA, Strecker MR, Wigger P (eds) The Andes – active subduction orogeny. Frontiers in Earth Science Series, Vol 1. Springer-Verlag, Berlin Heidelberg New York, pp 125–146, this volume

Husson L, Sempere T (2003) Thickening the Altiplano crust by gravity-driven crustal channel flow. Geophys Res Lett 30: doi 10.1029/2002GL016877

Hyndman RD, Currie CA, Mazzotti SP (2005) Subduction zone backarcs, mobile belts, and orogenic heat. GSA Today 15:4–10

Isacks BL (1988) Uplift of the Central Andean plateau and bending of the Bolivian orocline. J Geophys Res 93:3211–3231

Kameyama M, Yuen DA, Karato SI (1999) Thermal-mechanical effects of low-temperature plasticity (the Peierls mechanism) on the deformation of a viscoelastic shear zone. Earth Planet Sci Lett 168:159–172

Kay RW, Kay SM (1993) Delamination and delamination magmatism. Tectonophysics 219:177–189

Kay SM, Mpodozis C, Coira B (1999) Neogene magmatism, tectonism and mineral deposits of the Central Andes (22° to 33° S) In: Skinner BJ (ed) Geology and ore deposits of the Central Andes. Soc Econ Geol Spec pub 7, pp 27–59

Khazaradze G, Klotz J (2002) Short- and long-term effects of GPS measured crustal deformation rates along the south Central Andes. J Geophys Res B108(6)

Kley J, Monaldi C (1998) Tectonic shortening and crustal thickness in the Central Andes: how good is the estimate? Geology 26:723–726

Kley J, Monaldi CR, Salfity JL (1999) Along-strike segmentation of the Andean foreland: causes and consequences. Tectonophysics 301:75–94

Klotz J, Abolghasem A, Khazaradze G, Heinze B, Vietor T, Hackney R, Bataille K, Maturana R, Viramonte J, Perdomo R (2006) Long-term signals in the present-day deformation field of the Central and Southern Andes and constraints on the viscosity of the Earth's upper mantle. In: Oncken O, Chong G, Franz G, Giese P, Götze H-J, Ramos VA, Strecker MR, Wigger P (eds) The Andes – active subduction orogeny. Frontiers in Earth Science Series, Vol 1. Springer-Verlag, Berlin Heidelberg New York, pp 65–90, this volume

Kopf A, Brown KM (2003) Friction experiments on saturated sediments and their implications for the stress state of the Nankai and Barbados subduction thrusts. Marine Geology 202(3–4):193–210

Koulakov I, Sobolev SV, Asch G (in press) P- and S-velocity images of the lithosphere-asthenosphere system in the Central Andes from local-source tomographic inversion. Geophys J Int

Lamb S, Davis P (2003) Cenozoic climate change as a possible cause for the rise of the Andes. Nature 425:792–797

Lamb S, Hoke L (1997) Origin of the high plateau in the Central Andes, Bolivia, South America. Tectonics 16:623–649

Lamb S, Hoke L, Kennan L, Dewey J (1997) Cenozoic evolution of the Central Andes in Bolivia and Northern Chile. In: Burg JP, Ford M (eds) Orogeny through time. Geol Soc Spec Publ 121, pp 237–264

Lucassen F, Becchio R, Harmon R, Kasemann S, Franz G, Trumbull R, Romer RL, Dulski P (2001) Composition and density model of the continental crust in an active continental margin – the Central Andes between 18° and 27° S. Tectonophysics 341:195–223

Lüth S, Wigger P (2003) A crustal model along 39° S from a seismic refraction profile ISSA2000. Rev Geol Chile 30(1):83–101

Mackwell SJ, Zimmerman ME, Kohlstedt DL (1998) High-temperature deformation of dry diabase with application to tectonics on Venus. J Geophys Res 103:975–984

McQuarrie N, De Celles P (2001) Geometry and structural evolution of the Central Andean backthrust belt, Bolivia. Tectonics 20(5): 669–692

Medvedev S, Podladchikov Y, Handy MR, Scheuber E (2006) Controls on the deformation of the Central and Southern Andes (10–35° S): insight from thin-sheet numerical modeling. In: Oncken O, Chong G, Franz G, Giese P, Götze H-J, Ramos VA, Strecker MR, Wigger P (eds) The Andes – active subduction orogeny. Frontiers in Earth Science Series, Vol 1. Springer-Verlag, Berlin Heidelberg New York, pp 475–494, this volume

Moresi LN, Dufour F, Muhlhaus HB (2003) A Lagrangian integration point finite element method for large deformation modeling of viscoelastic geomaterials. J Comp Phys 184:476–497

Oncken O, Hindle D, Kley J, Elger K, Victor P, Schemmann K (2006) Deformation of the central Andean upper plate system – facts, fiction, and constraints for plateau models. In: Oncken O, Chong G, Franz G, Giese P, Götze H-J, Ramos VA, Strecker MR, Wigger P (eds) The Andes – active subduction orogeny. Frontiers in Earth Science Series, Vol 1. Springer-Verlag, Berlin Heidelberg New York, pp 3–28, this volume

Pardo Casas F, Molnar P (1987) Relative motion of the Nazca (Farallon) and South American plates since Late Cretaceous time. Tectonics 6:233–248

Peacock S (1996) Thermal and petrologic structure of subduction zones. In: Bebout G, et al. (eds) Subduction, top to bottom. AGU Geophys Monogr Ser 96, Washington DC, pp 119–134

Petrunin A, Sobolev SV (2005) What controls thickness of sediments and lithospheric deformation at a pull–apart basin? Geology 34:389–392

Poli S, Schmidt MW (2002) Petrology of subducted slabs. Ann Rev Earth Planet Sci 30:207–235

Poliakov AN, Cundall PA, Podladchikov YY, Lyakhovsky VA (1993) An explicit inertial method for the simulation of the viscoelastic flow: an evaluation of elastic effects on diapiric flow in two- and three-layers models. In: Stone DB, Runcorn SK (eds) Flow and creep in the Solar System: observations, modelling and theory. Kluwer Academic Publishers, pp 175–195

Pope DC, Willett SD (1998) Thermo-mechanical model for crustal thickening in the Central Andes driven by ablative subduction. Geology 26:511–514

Ranero CR, Phipps Morgan J, McIntosh K, Relchert C (2003) Bending-related faulting and mantle serpentinization at the Middle America trench. Nature 425:367–373

Royden LH, Burchfiel BC, King RW, Wang E, Chen Z, Shen F, Liu Y (1997) Surface deformation and lower crustal flow in eastern Tibet. Science 276:788–790

Russo R, Silver PG (1996) Cordillera formation, mantle dynamics, and the Wilson cycle. Geology 24:511–514

Rybacki E, Dresen G (2000) Dislocation and diffusion creep of synthetic anorthite aggregates. J Geophys Res 105:26017–26036

Scheuber E, Bogdanic T, Jensen A, Reutter K-J (1994) Tectonic development of the north Chilean Andes in relation to plate convergence and magmatism since the Jurassic. In: Reutter K-J, Scheuber E, Wigger P (eds) Tectonics of the Southern Central Andes. Springer-Verlag, Berlin Heidelberg New York, pp 121–139

Silver PG, Russo RM, Lithgow–Bertelloni C (1998) Coupling of South American and African plate motion and plate deformation. Science 279:60–63

Sobolev SV, Babeyko AY (1994) Modeling of mineralogical composition, density and elastic wave velocities in anhydrous magmatic rocks. Survey Geophys 15:515–544

Sobolev SV, Babeyko AY (2005) What drives orogeny in the Andes? Geology 33:617–620

Sobolev SV, Zeyen H, Stoll G, Werling F, Altherr R, Fuchs K (1996) Upper mantle temperatures from teleseismic tomography of French Massif Central including effects of composition, mineral reactions, anharmonicity, anelasticity and partial melt. Earth Plan Sci Lett 139:147–163

Sobolev SV, Petrunin A, Garfunkel Z, Babeyko AY, DESERT Group (2005) Thermo-mechanical model of the Dead Sea transformation. Earth Planet Sci Lett 238:78–95

Somoza R (1998) Updated Nazca (Farallon)-South America relative motions during the last 40 My: implications for mountain building in the Central Andean region. J S Am Earth Sci 11:211–215

Springer M, Förster A (1998) Heat flow density across the Central Andean subduction zone. Tectonophysics 291:123–139

Sulsky D, Zhou SJ, Schreyer HL (1995) Application of a particle-in-cell method to solid mechanics. Comput Phys Commun 87:236–252

Tassara A (2005) Interaction between the Nazca and South American plates and formation of the Altiplano-Puna plateau: Review of a flexural analysis along the Andean margin (15°–34° S). Tectonophysics 399:39–57

Trumbull RB, Riller U, Oncken O, Scheuber E, Munier K, Hongn F (2006) The time-space distribution of Cenozoic volcanism in the South-Central Andes: a new data compilation and some tectonic implications. In: Oncken O, Chong G, Franz G, Giese P, Götze H-J, Ramos VA, Strecker MR, Wigger P (eds) The Andes – active subduction orogeny. Frontiers in Earth Science Series, Vol 1. Springer-Verlag, Berlin Heidelberg New York, pp 29–44, this volume

Victor P, Oncken O, Glodny J (2004) Uplift of the western Altiplano Plateau: evidence from the Precordillera between 20° S and 21° S, Northern Chile. Tectonics 23: doi 10.1029/2003TC001519

Vietor T, Echtler H (2006) Episodic Neogene southward growth of the Andean subduction orogen between 30° S and 40° S – plate motions, mantle flow, climate, and upper-plate structure. In: Oncken O, Chong G, Franz G, Giese P, Götze H-J, Ramos VA, Strecker MR, Wigger P (eds) The Andes – active subduction orogeny. Frontiers in Earth Science Series, Vol 1. Springer-Verlag, Berlin Heidelberg New York, pp 375–400, this volume

von Hunen J, van den Berg AP, Vlaar NJ (2004) Various mechanisms to induce shallow flat subduction: a numerical parameter study. Phys Earth Planet Int 146:179–194

Whitman D, Isacks BL, Kay SM (1996) Lithospheric structure and along-strike segmentation of the Central Andean Plateau: seismic Q, magmatism, flexture, topography and tectonics. Tectonophysics 259:29–40

Yañez G, Cembrano J (2004) Role of viscous plate coupling in the late Tertiary Andean tectonics. J Geophys Res 109(2):1–21

Yuan X, Sobolev SV, Kind R, Oncken O, et al. (2000)Subduction and collision processes in the Central Andes constrained by converted seismic phases. Nature 408:958–961

Yuan X, Sobolev SV, Kind R (2002) New data on Moho topography in the Central Andes and their geodynamic implications. Earth Planet Sci Lett 199:389–402

Supplementary DVD

Animation 1 (AVI). Break-up of the slab due to high interplate friction coefficient (0.10). Colors represent rock types and arrows show velocity vectors. At $t = 3$ Myr the slab (*blue*) breaks off. The similar picture is observed at interplate friction coefficients higher than 0.10.

Animation 2 (AVI). Evolution of structure for the Central Andes' model. Colors represent rock types.

Animation 3 (AVI). Evolution of density for the Central Andes' model.

Animation 4 (AVI). Evolution of temperature for the Central Andes' model. Arrows show velocity vectors.

Animation 5 (AVI). Evolution of finite strain (high strain – *red*) for the thin-skin deformation model.

Animation 6 (AVI). Evolution of finite strain (high strain – *red*) for the thick-skin deformation model.

Animation 7 (PDF). Sequence of snapshots showing simultaneous evolution of upper-plate shortening rate, crustal and mantle temperatures and magnetic activity for the version of the Central Andes' model.